SAMICOS Determines Mitochondrial Cristae Architecture by Mediating Mitochondrial Outer and Inner Membrane Contact

Junhui Tang[1,#], Kuan Zhang[1,#,3], Jun Dong[1], Chaojun Yan[1], Shi Chen[2], and Zhiyin Song[1,*]

[1]Hubei Key Laboratory of Cell Homeostasis, College of Life Sciences, Wuhan University, Wuhan, Hubei, 430072, China.

[2]Key Laboratory of Combinatorial Biosynthesis and Drug Discovery, Ministry of Education, School of Pharmaceutical Sciences, Medical Research Institute, Wuhan University, Hubei, China.

[3] current address: Cardiovascular Research Institute, University of California, San Francisco, San Francisco, United States

[#] Co-first author.

* Correspondence to Zhiyin Song: songzy@whu.edu.cn

ABSTRACT

Mitochondrial cristae are critical for efficient oxidative phosphorylation, however, how cristae architecture is precisely organized remains obscure. Here, we discovered that SAM complex directly interacts with MICOS complex to form a supercomplex, SAMICOS, which bridges mitochondrial outer- and inner-membrane by Sam50-Mic19-Mic60 axis. Mic19, a core component of MICOS, establishes mitochondrial outer- and inner-membrane contact by directly interacting with Sam50 and Mic60, and is required for the assembly of SAMICOS by stabilizing and connecting SAM and MICOS. Interestingly, Mic19 is cleaved by mitochondrial protease OMA1 upon mitochondrial stresses. The cleavage of Mic19 leads to SAMICOS disruption, which causes abnormal mitochondrial morphology, loss of crista junctions, and reduced ATP production even in the presence of SAM and MICOS. Importantly, Sam50 acts as an anchoring point at mitochondrial outer-membrane to guide formation of mitochondrial crista junctions. Therefore, we propose a model that SAM complex integrates with MICOS complex to regulate mitochondrial cristae architecture.

INTRODUCTION

Mitochondria are fully articulated and highly organized organelles which surrounded by two membranes: the outer mitochondrial membrane (OMM) and the inner mitochondrial membrane (IMM) (Mannella, 2006). The outer membrane is the first interface and barrier for mitochondria to communicate the substance, energy and information with the cytosol (Wenz et al., 2014). The outer membrane possesses a dedicated protein import system, including TOM complex, the translocase of the outer mitochondrial membrane, and SAM complex, the mitochondrial sorting and assembly machinery (Hohr et al., 2015; Kozjak et al., 2003; Wenz et al., 2014). The inner membrane is consist of the inner boundary membrane (IBM) and the cristae membrane (CM). The IBM is closely apposed to the OMM while the inner membrane protrudes from the IBM into the inner space of the mitochondria formed cristae membrane (Demongeot et al., 2007; Huynen et al., 2016; van der Laan et al., 2016). Cristae membranes are large tubular invaginations and are thought to increase the local charge density/pH to enhance ATP synthesis via oxidative phosphorylation (Hoppins et al., 2011). The connections between IBM and the cristae are the crista junctions (CJs) which is relatively uniform narrow, tubular and slot-like structures (Rabl et al., 2009).

Cristae and crista junctions are important for mitochondrial organization and function (Zick et al., 2009). Lots of experimental results revealed that the formation of cristae and crista junctions requires Mgm1 (known as OPA1 in mammals), the dimeric form of the F1FO-ATP synthase (F1FO), the MICOS (mitochondrial contact site and cristae organizing system) complex, and Prohibitins (PHBs) (Harner et al., 2016b; Rabl et al., 2009). Mgm1, the dynamin-like fusion protein of IMM, mediates the fusion of IMM, it cooperates with dimeric F1FO to stabilize the cristae membranes and to thereby generate the sac-like structure. Assembly of the MICOS complex is proposed to limit the fusion process by forming a crista junction (Harner et al., 2016b; Huynen et al., 2016; Pfanner et al., 2014; Zick et al., 2009). Prohibitins exist as two closely related proteins (PHB1 and PHB2) that localize to the IMM (Merkwirth et al., 2008). PHBs were reported to assemble into ring-like structures that provide a frame-work to stabilize the structure of crista (Harner et al., 2016b; Merkwirth et al., 2008; Semenzato et al., 2011). However, So far, how mitochondrial cristae and crista junctions are formed remains an ambiguous question.

Eight subunits of MICOS complex in mammalian are described: Mic60/IMMT, Mic19/CHCHD3, Mic10/MINOS1, Mic23/Mic26/APOO, Mic27/APOOL, Mic13/QIL1,

Mic25/CHCHD6 and Mic14/CHCHD10. Mic19 and Mic25 are peripheral membrane protein whereas others are transmembrane protein containing at least one transmembrane domain (Alkhaja et al., 2012; An et al., 2012; Darshi et al., 2011; Genin et al., 2016; Guarani et al., 2015; Koob et al., 2015; Li et al., 2016; Rampelt et al., 2017; Weber et al., 2013) . In this complex, Mic60, Mic19, and Mic10 play a dominant role in cristae membrane structure. That is mainly because of missing any one of these subunits, especially Mic60 and Mic10, will generate more severe cristae phenotype (Bohnert et al., 2015; Li et al., 2016). Not only in maintaining cristae architecture, MICOS subunits also possess other capacity: Mic60 and Mic10，two mitochondrial inner membrane proteins, show the ability in bending the liposome membrane in vitro (Barbot et al., 2015; Hessenberger et al., 2017), Mic60 and Mic19 ablation can affect the mitochondrial dynamics (Cho et al., 2017; Darshi et al., 2011; Li et al., 2016). Mediating mitochondrial contact sites formation is another feature of MICOS complex (Harner et al., 2011). Mic60, Mic19, and Mic25 which are responsible for the formation of OMM and IMM contact sites are reported in mammalian system and all of them have the potential to bind to the outer membrane protein Sam50 (An et al., 2012; Darshi et al., 2012; Sastri et al., 2017). Existing study showed that Sam50, the central component of SAM complex, was also a specific MICOS interaction partner and also play important role in the maintenance of the structure of cristae. Cells missing Sam50 display severe mitochondrial morphology and cristae phenotype (Capala et al., 2016; Ott et al., 2012). However, it remains not fully understood how the synergistic interactions between SAM and MICOS complex play role in the formation of contact sites and the biogenesis of mitochondrial cristae structure.

In this study, we reported that SAM complex directly interacts with MICOS complex to form a supercomplex, SAMICOS. Mic19 dominantly mediates the interaction between SAM and MICOS, and is required for the assembly and stabilization of SAMICOS. We find that Mic19 can be cleaved at N-terminal by mitochondrial metalloprotease OMA1 after Sam50 depletion or Mic19 overexpression. The cleaved short form of Mic19 (S-Mic19) disrupts the contact between SAM and MICOS and then causes the abnormal mitochondrial morphology and loss of mitochondrial crista junctions, moreover, impairs ATP production. We also put forward the notion that SAM complex can serve as an anchoring point in OMM for the formation of mitochondrial cristae junction. Moreover, Mic25, an important paralog of Mic19, can act as reserves to rescue the interaction between Sam50 and Mic60. In addition, overexpressed Mic25 in Mic19 knockout cells can reconstruct the mitochondrial morphology

and crista junctions. Overall, we provide a new mode that OMM and IMM contact regulates the formation of cristae junction.

RESULTS

Mic19 stabilizes SAM and MICOS complexes and bridges SAM and MICOS to form a supercomplex SAMICOS

Mic19, one central subunit of MICOS complex, plays an essential role in maintaining cristae architecture integrity and mitochondrial function (Darshi et al., 2011; van der Laan et al., 2012). To further investigate the comprehensive role of Mic19, we used 293T cells transiently expressing Mic19-Flag to perform co-immunoprecipitation (co-IP) experiments and identify Mic19 binding proteins by Tandem mass spectrometry (MS/MS). MS/MS data (Table S1) showed a number of proteins that may exist in the same complex. In order to confirm the MS/MS data, the co-IP assay and followed immunoblotting revealed that Mic19 interacted with Sam50 (the key component of SAM complex), Mic60 (the core subunit of MICOS), and Mic25 (Figure 1A). We also performed GST-pull down assay to check whether these interactions are direct. Mic19 indeed directly interacted with Sam50 or Mic60 but not Mic25 (Figures 1B, 1C, and S1A). Because Mic19 is a core component of MICOS and directly interacts with Mic60 and Sam50, we then examine whether Mic19 depletion affects the integrity of MICOS and SAM complex. We generated Mic19 knockout (KO) HeLa cell line by using CRISPR/Cas9 system mediated genome editing. Immunoblotting revealed that Mic19 knockout not only resulted in a remarkable decrease of Sam50, Metaxin 1 (MTX1), and Metaxin 2 (MTX2) (the subunits of SAM complex), but also markedly reduced Mic60 and Mic10 (the subunits of MICOS complex) (Figure 1D), but did not affect the level of Mic25 (Figure 1D). These results hinted that Mic19 could simultaneously stabilize SAM and MICOS complexes. To rule out the off-target effects of CRISPR/Cas9 system, we reintroduced Mic19$^{\Delta gRNA}$-Flag intoMic19-KO HeLa cells (ΔgRNA represents mutated in gRNA targeting site, without altering the amino acid sequence, in order to prevent gRNA binding to the exogenous Mic19). Immunoblotting revealed that the levels of a series of proteins, which are reduced by Mic19 KO, were recovered to the normal levels in Mic19-Flag expressed Mic19-KO cells (Figure 1E). In addition, Mic10 or Mic25 knockout had no effect on SAM complex subunits (Sam50, Metaxin 1, and Metaxin2) and the other MICOS complex components (Mic60, Mic19 etc.) (Figures S1B and S1C). Furthermore, Sam50 knockdown (short-hairpin mediated RNA interference, shSam50) caused

depletion of Metaxin 1 and Metaxin 2, which are its partner in SAM complex, but did not affect Mic60, Mic10, and Mic25 (Figure S1D). These results suggested that only Mic19 play a key role in concurrently protecting SAM and MICOS complexes.

To further illustrate the role of Mic19 in connecting SAM and MICOS complexes, we analyzed mitochondria from WT cells (lane 1), Mic19-KO cells (lane 2), and Mic19-KO regained Mic19-Flag cells (lane 3) by blue native polyacrylamide gel electrophoresis (BN-PAGE). Antibodies against Mic19 or Mic60 specifically recognized two protein complexes in lane 1 and lane 3 (Figure 1F). One complex showed a pronounced maximum at around 700kDa, referencing to existing study (Huynen et al., 2016), this complex is MICOS because it could not be detected by anti-Sam50 antibody. The other is at about 2000kDa and contains MICOS and SAM complex because it could be detected by anti-Mic19, anti-Mic60, or anti-Sam50 antibodies (Figure 1F), thus, we named this supercomplex 'SAMICOS'. SAMICOS may contain 2 SAM and MICOS complexes or some other proteins according to its molecular weight. In addition, the bottom complexes (~250kDa or 125kDa) recognized by anti-Sam50 antibody are SAM complex or unidentified complex containing Sam50. However, MICOS, SAM, or SAMICOS complex was not detected after Mic19 depletion (lane 2). In order to verify the credibility of the results, we performed BN-PAGE assay using heart- or liver-specific deficiency of Mic19 mouse mitochondria. Similarly, SAM, MICOS, or SAMICOS complex was depolymerized upon Mic19 deficiency in heart or liver (Figures 1G and S1E). These results indicate that Mic19 depletion results in the dissociation of the SAM complex and MICOS complex, and constituent subunits also are degraded after dissociating from the complex. Therefore, Mic19 bridges SAM and MICOS to form a supercomplex SAMICOS and is responsible for the stabilization of SAM, MICOS, and SAMICOS complexes.

Mic19 detached from SAMICOS complexes can be cleaved at N-terminal by mitochondrial protease OMA1

Most of the mitochondrial proteins dissociated from the complex are degraded by mitochondrial proteases (Quiros et al., 2013; Ruan et al., 2013). Our previous works have shown that Mic60 degradation, caused by down-regulation of Mic19, is mediated by the mitochondrial protease Yme1L (Li et al., 2016). Mic19 depletion also leads to the degradation of Sam50 (Figure 1D), therefore, we test whether Sam50 degradation is mediated by Yme1L. Yme1L knockdown inhibited Mic19 knockdown-induced degradation of Sam50 (Figure S2A), furthermore, Yme1L

physically interacted with Sam50 (Figure S2B). These data demonstrate that Yme1L regulates Sam50 degradation. Because Sam50 directly binds to Mic19 (Figures 1A and 1B), we examine whether Sam50 is related to Mic19 degradation. To our surprise, instead of causing degradation of Mic19, Sam50 knockdown (shSam50) resulted in the cleavage of Mic19, and formed a short form of Mic19 (S-Mic19) (Figure 2A). However, the depletion of Mic60 or Mic25 did not induce Mic19 cleavage (Figures S2C and S2D). Next, considering that Mic19 is a mitochondrial intermembrane space protein, we investigated whether mitochondrial inner membrane protease Yme1L or OMA1 is responsible for the cleavage of Mic19. Mic19 was cleaved in Yme1L knockout but not in OMA1 knockout cells (Figures 2A and 2B), suggesting that OMA1 regulates Mic19 cleavage.

To determine whether the Mic19 cleavage locates at the N-terminus or C-terminus, Mic19-Flag (Flag tag at the C-terminus) was transiently overexpressed in 293T cells. Unexpectedly, the cleavage of Mic19-Flag was also detected (Figure S2E). Due to little endogenous Mic19 cleavage in wild-type cells, we speculate that excessive Mic19-Flag, caused by transient expression, may not be completely assembled to SAMICOS complex, and leaving unassembled Mic19 or Mic19-Flag is then cleaved by OMA1. To examine our hypothesis, we built the Mic19-Flag stably overexpressed HeLa cells and treated cells with CCCP (an oxidative phosphorylation inhibitor, capable of reducing mitochondrial membrane potential and activating OMA1 metalloprotease activity (Zhang et al., 2014)). As we expected, both endogenous S-Mic19 and exogenous S-Mic19-Flag were detected in CCCP-treatment group (Figure 2C), implying unassembled Mic19 can be cleaved at N-terminal. In contrast, in response to OMA1 knockdown (in HeLa cells) or OMA1 knockout (in MEFs), overexpressed Mic19-Flag failed to be cleaved even after CCCP treatment (Figures 2D and S2F). In addition, co-immunoprecipitation assay revealed that Mic19 interacted with OMA1^{E324Q}, a mutation that only blocks the OMA1 protease activity (Baker et al., 2014) (Figure 2E). These results demonstrated that Mic19 is cleaved at N-terminal by mitochondrial protease OMA1 in response to Sam50 downregulation or CCCP treatment.

To ascertain the cutting site of Mic19, we first compared the molecular weight of proteins being displayed in SDS-PAGE, and got an around 3kD size difference that is equivalent to 36 amino acids on average. We then picked up the adjacent 20 amino acids, residues26-39aa in human Mic19, to examine the evolutional conservation. Alignment of this short amino acid sequence from different species showed that this region (26–39aa) of Mic19 is highly

evolutionarily conserved (Figure S2G). We then deleted 31-40aa of Mic19 and found the N-terminal processing of Mic19 is terminated after CCCP treatment (Figure 2G). Interestingly, through the alignment, Mic25, another MICOS subunit, is about 90 percent homologous with Mic19 in this twenty amino acid sequence, and only two amino acids 'VN' of Mic25 is different from that in Mic19 (Figure 2F). Meanwhile, we searched the downstream sequence right after the site number 39 and found that Mic19 protein sequence in some species (like Equus caballus) starts from site 36 of human Mic19 right behind the two un-conserved amino acids (Figure S2G). The un-conserved character within this sequence indicates that these two amino acids may be critical for cleavage of Mic19. Importantly, exogenous Mic25-Flag is un-cleavable upon CCCP treatment (Figure 2H), so we mutated 'ID' in Mic19 to 'VN' ($Mic19^{ID33\text{-}34VN}$) and implemented in a manner similar as control did (Figure 2G). No cleavage at the N-terminal of $Mic19^{ID33\text{-}34VN}$ was detected (Figure 2G), indicating that amino acids 'ID' of Mic19 is the site of cleavage. To eliminate the possibility that this two amino acids are important for OMA1 binding but not cleavage, we co-expressed Mic19-Flag or $Mic19^{ID33\text{-}34VN}$-Flag with $OMA1^{E324Q}$-Myc in 293T cells, co-immunoprecipitation assay and followed immunoblotting revealed that both Mic19-Flag and $Mic19^{ID33\text{-}34VN}$-Flag interacted with $OMA1^{E324Q}$-Myc (Figures S2H), demonstrating that 'ID' is OMA1 cleavage site but not binding site. To further test whether two amino acids are indispensable for the OMA1 cleavage, we replaced the 'VN' in Mic25 with 'ID' ($Mic25^{VN35\text{-}36ID}$) and examined the processing of $Mic25^{VN35\text{-}36ID}$. OMA1-cleavable form of $Mic25^{VN35\text{-}36ID}$ was displayed (Figures 2I and 2J). Therefore, the inter-paralog replacement of two amino acids endows Mic19 obvious resistance and Mic25 more susceptible to OMA1 cleavage. Overall, the processing site of Mic19 by OMA1 is right after the 'ID' at its N terminal.

The interaction between Mic19 and Sam50 is required for the integrity of SAMICOS complex

To explore the function of Mic19 cleavage, we firstly investigated whether Mic19 cleavage affects the interactions between Mic19 and other proteins. Co-immunoprecipitation (co-IP) assay and GST-pull down assay revealed that S-Mic19-Flag but not Mic19 (1-35aa)-Flag (N-terminal 35 amino acids of Mic19) directly interacted with Mic60, and Mic19 (1-35aa)-Flag but not S-Mic19-Flag specifically binds to Sam50 (Figures 3A-3D). These results demonstrated that Mic19 stretches out its N-terminal to physically interact with Sam50, leaving its CHCH

domain directly binding to the Mic60. Thus, the interaction between Mic19 and Sam50 was disrupted after Mic19 cleavage by OMA1. We then examined the effect of disrupted interaction between Mic19 and Sam50 on SAMICOS complex. We reintroduced the Mic19$^{\Delta gRNA}$-Flag, S-Mic19$^{\Delta gRNA}$-Flag or Mic19 $^{(ID33-34VN)\ \Delta gRNA}$-Flag in Mic19 KO HeLa cells. Mitochondria from WT cells, Mic19 KO cells, Mic19$^{\Delta gRNA}$-Flag cells or S-Mic19$^{\Delta gRNA}$-Flag expressed Mic19 KO cells were then analyzed by BN-PAGE. SAMICOS complex was detected in WT (lane 1) or Mic19$^{\Delta gRNA}$-Flag expressed Mic19 KO cells (lane 3) but not in Mic19 KO (lane 2) or S-Mic19$^{\Delta gRNA}$-Flag expressed Mic19 KO cells (lane 4) (Figure 3E). Interestingly, MICOS complex (~700kDa) were still maintained in S-Mic19$^{\Delta gRNA}$-Flag expressed Mic19 KO cells (Figure 3E), suggesting that S-Mic19 is enough for assembly of MICOS complex. In addition, immunoblotting revealed that MICOS subunits Mic60 and Mic10 were recovered in Mic19$^{\Delta gRNA}$-Flag, Mic19 $^{(ID33-34VN)\ \Delta gRNA}$-Flag and S-Mic19$^{\Delta gRNA}$-Flag expressed-Mic19 KO cells (Figure 3F). However, Sam50 was only recovered in Mic19$^{\Delta gRNA}$-Flag and Mic19 $^{(ID33-34VN)\ \Delta gRNA}$-Flag but not in S-Mic19$^{\Delta gRNA}$-Flag expressed Mic19 KO cells (Figure 3F), suggesting that SAMICOS is disrupted in S-Mic19$^{\Delta gRNA}$-Flag expressed-Mic19 KO cells because of the disappearance of Sam50. Therefore, the interaction between Mic19 and Sam50 is required for the integrity of SAMICOS complex.

SAMICOS complex is critical for the maintenance of normal mitochondrial morphology, mitochondrial crista junctions, and ATP production

To investigate the role of SAMICOS in mitochondrial morphology and structure, Mic19$^{\Delta gRNA}$-Flag, S-Mic19$^{\Delta gRNA}$-Flag or Mic19 $^{(ID33-34VN)\ \Delta gRNA}$-Flag was expressed in Mic19 KO HeLa cells. Mitochondrial morphology of cells stably expressing mitochondrial matrix-targeted GFP (Mito-GFP) was visualized by confocal microscopy. Remarkably, almost all the Mic19 KO HeLa cells showed the 'Expanded and spherical', but not fragmented, mitochondrial network (Figure 4A): thicker mitochondria form the 'head' and the rest normal mitochondria are the 'tail'. After re-expression of Mic19$^{\Delta gRNA}$-Flag or Mic19 $^{(ID33-34VN)\ \Delta gRNA}$-Flag in Mic19 KO cells, which results in restoration of SAMICOS complex, the normal tubular mitochondria morphology were recovered (Figures 4A and 4B). Surprisingly, some 'large spherical mitochondria' appeared in S- Mic19$^{\Delta gRNA}$- Flag expressed-Mic19 KO cells in which MICOS is restored but SAMICOS is not recovered (Figures 4A and 4B), indicating that SAMICOS regulates mitochondrial morphology. We previously reported that mitochondria in Mic60 or

Sam50 knockdown cells became 'large sphere' (Jian et al., 2018; Li et al., 2016). The appearance of large spherical mitochondria in shMic60, shSam50, or S-Mic19$^{\Delta gRNA}$-Flag cells indicates that this specific mitochondrial morphology is probably due to the disrupted interaction between Mic19 and Sam50.

We and others have shown that MICOS complex key subunits, especially Mic60 and Mic10, can affect mitochondrial cristae conformation (Alkhaja et al., 2012; Li et al., 2016). Since Mic60 and Mic10 expression were recovered in S-Mic19$^{\Delta gRNA}$-Flag expressed Mic19 KO cells, we speculated that cristae phenotype should be normal. However, the crista junctions, analyzed by TEM, were disappeared in S-Mic19$^{\Delta gRNA}$-Flag expressed Mic19 KO cells compared with WT or Mic19$^{\Delta gRNA}$-Flag expressed Mic19 KO cells (Figure 4C).

To further rule out the possibility that the decrease of Sam50 resulted in the disappearance of crista junctions (CJs) in S-Mic19$^{\Delta gRNA}$-Flag expressed Mic19 KO cells, we next re-introduced Sam50 into S-Mic19$^{\Delta gRNA}$-Flag expressed Mic19 KO cells to directly confirm the role of interaction between Mic19 and Sam50 in cristae patterning. Compared with S-Mic19$^{\Delta gRNA}$-Flag alone, S-Mic19$^{\Delta gRNA}$-Flag and Myc-Sam50 co-expressed Mic19 KO cells maintained Sam50, Mic60 and Mic10 expression (Figure S3A), but still could not restore crista junctions (CJs) (Figures 4C and 4D); in addition, mitochondrial morphology in the co-expressed cells still showed 'large sphere' (Figures S3B and S3C). Furthermore, BN-PAGE assays revealed that S-Mic19$^{\Delta gRNA}$-Flag and Myc-Sam50 co-expressed Mic19 KO cells still loss SAMICOS complex although they maintained SAM and MICOS complexes (Figure 4E). We also investigate the role of SAMICOS complex in energy metabolism. Disrupted SAMICOS, even in the presence of SAM and MICOS complex (Figure 4E), resulted in significantly reduced ATP production (Figure 4F). Therefore, SAMICOS assembled by interaction of Mic19 and Sam50 is indispensable for regulation of mitochondrial morphology, crista junctions (CJs) formation, and ATP production.

Sam50 acting as an anchoring point in mitochondrial outer membrane is required for formation of mitochondrial crista junctions

Sam50 acting as the N-terminal binding protein of Mic19, just like a cap, protects the N-terminus of Mic19 from mitochondrial proteases in order to maintain the intact of Sam50-Mic19-Mic60 axis. So as the representative of the outer membrane protein, what is the role of Sam50 in the formation of crista junctions? We take short-time depleted Sam50 strategies, and

to rule out the possibility that the cleavage of Mic19 is the primary effect leading to cristae deformation, we performed Sam50 knockdown (shSam50) in WT cells, Mic19$^{\Delta gRNA}$-Flag or Mic19 $^{(ID33\text{-}34VN)\ \Delta gRNA}$-Flag expressed Mic19 KO cells, respectively. In response to shSam50, Mic60 and Mic10 were unaltered no matter whether Mic19 is cleaved or not (Figure 5A). Mitochondrial morphology in above cell lines was also measured by confocal microscopy. All the cell lines depleting Sam50 (shSam50, 5days) showed remarkably fragmented mitochondria (Figures 5B and 5C). These results suggest that Sam50 directly regulates mitochondrial morphology. Mitochondrial cristae remodeling was then examined by transmission electron microscope (TEM). Most of cristae in WT mitochondria connected with inner membrane and presented regularly arranged (Figure 5D); however, almost all cristae of shSam50 mitochondria pinched off from the inner membrane, leading to crista junctions collapsed (Figure 5E). The similar crista were also found in shSam50 plus Mic19$^{\Delta gRNA}$-Flag or Mic19 $^{(ID33\text{-}34VN)\ \Delta gRNA}$-Flag expressed Mic19 KO cells (Figures 5E and 5F). These results indicate that Sam50 may act as an anchoring point in mitochondria outer membrane for crista junctions. To further verified this hypothesis, Flag-Sam50 stably expressed in COS7 cells were analyzed by using stimulated emission depletion microscopy (STED) techniques. Distribution of Flag-Sam50 on the mitochondrial outer membrane are dotted (Figure 5G), importantly, the location of about 30% Sam50 are over against to crista junctions (Figure 5H).Therefore, Sam50 may serve as an anchoring point for MICOS complex, and SAM connect MICOS through the sam50-Mic19-Mic60 axis to anchor the crista junctions at a specific site of mitochondrial inner membrane.

Restoration of Sam50-X-Mic60 axis by overexpression of Mic25 in Mic19 KO cells can reconstruct mitochondrial crista junctions and recover ATP production

Since the Sam50-Mic19-Mic60 axis plays a decisive role in the maintenance of mitochondrial morphology and structure. Destroying either of three subunits can disrupt the axis, however, only Mic60 knockdown (Li et al., 2016) or Sam50 depletion (Jian et al., 2018), but not Mic19 knockout, induced large spherical mitochondria (Figures 4A, S4A and S4B), suggesting that there may be another component (called X) which can replace Mic19 to form Sam50-X-Mic60 axis after Mic19 knockout. Of all the subunits in the MICOS complex, only Mic25 has this possibility as a candidate, because Mic25 is the only MICOS subunit that exhibits 36% overall sequence identity and 80% similarity to Mic19 (Zerbes et al., 2012). In addition, Mic60 depletion reduced Mic25, while Mic19 knockout just decreased Mic60 but not altering Mic25

level (Figure 6A). Moreover, Mic25 is also capable of forming direct interaction with Sam50 and Mic60 (Figures 6B and 6C). Therefore, we investigate whether there is functional overlap between Mic19 and Mic25. We firstly depleted Mic25 in WT or Mic19 KO cells to examine the functional overlap in the maintenance of mitochondrial morphology. Mic25 knockout did not affect the level of other MICOS subunits and mitochondrial morphology (Figures 6D and S4C). However, the depletion of Mic25 (shMic25) in Mic19 KO cells caused mitochondria shape converting to 'large spherical' (Figures 6E and 6G), and led to an obvious further reduction of Mic60, Mic10 and Sam50 (Figure S4C). Similar phenotype was recurrence when we disrupted Mic19 (shMic19) in Mic25 KO cells (Figures 6F, 6G, and S4C). These results demonstrate that Mic25 functionally overlap with Mic19, but Mic19 play a dominant role in mediating Sam50-X-Mic60 axis. Because Mic19 dominant Sam50-X-Mic60 axis, we then investigated whether Mic19 protein abundance is much higher than that of Mic25. We compared the relative protein levels of Mic19 and Mic25 in cells by comparing normalized Mic19-Flag with normalized Mic25-Flag. The level of endogenous Mic19 and Mic25 are comparable, and Mic25 only slightly lower (Figures S4D-S4G), which further confirmed that Mic19 dominants Sam50-X-Mic60 axis. In addition, Mic25 KO cells display normal mitochondrial cristae architecture (Figure S4H and S4I), suggesting that Sam50-Mic19-Mic60 axis plays a key role in mitochondrial cristae organization. Therefore, under normal conditions, Sam50-Mic19-Mic60 axis mainly exist; after Mic19 knockout, the unaffected Mic25 works together with the rest Mic60 and Sam50, and forms Sam50-Mic25-Mic60 axis to partially maintain the function of Sam50-X-Mic60 axis.

Since Mic25 can act as 'spare bearing', we investigated whether overexpressed Mic25 in Mic19 KO cells can form dominant axis to restore the mitochondrial outer and inner membrane contact. Overexpressed Mic25-Flag (about 10 fold of endogenous Mic25) in Mic19 KO cells recovered normal mitochondrial morphology (Figures 6H-6J). In addition, the level of other MICOS subunits was also recovered in Mic19 KO cells overexpressing Mic25-Flag (Figure 6J). These results suggested that overexpressed Mic25 can fill the position of Mic19 to form a new dominant axis with Sam50 and Mic60, and the new formed Sam50-Mic25-Mic60 axis can also reconnected the SAMICOS complex depolymerized by Mic19 depletion. Then, we examined whether overexpression of Mic25 can reshape the ultrastructure of mitochondria. Mitochondrial crista junctions reconstructed in Mic25 overexpressed Mic19 KO cells (Figures 6K and 6L). Moreover, Mic19 KO resulted in reduced ATP level, but ATP were recovered to normal level in

Mic25 overexpressed Mic19 KO cells (Figure 6M). Therefore, our data indicate that Mic25 is a compensatory factor for assembling SAMICOS complex, which bridges mitochondrial outer and inner membrane contact and regulates mitochondrial morphology and ultrastructure.

The model of mitochondrial cristae organization

Based on previous reports and our findings, we formulate a theoretical model to illustrate mitochondrial cristae organization and the de novo formation of crista junctions (Figure 7):

A. When de novo cristae formed, monomeric F1FO assembled into dimeric F1FO providing positive curvature to crista membranes (Davies et al., 2012; Harner et al., 2016a). At the same time, Mic60 targets to inner membrane forming an anchor site, which is called nucleation, to recruit other MICOS subunits including Mic19, Mic10, and Mic25. Mic10 oligomerization can bend mitochondrial inner membranes and then stretch the mitochondrial inner membrane toward the matrix (Barbot et al., 2015). Mic19 directly binding to Mic60, stretches out its N-terminal to physically interact with Sam50, and then close the distance between MICOS and SAM complex to form the contact site of mitochondrial outer- and inner-membrane. OPA1 oligomerization can be used to regulate the contraction of the cristae junction (CJ) (Barrera et al., 2016; Harner et al., 2016b; Hering et al., 2017). In the end, curvature and fusion of inner membranes is halted when integrated SAMICOS complex is formed, meanwhile, CJ is generated.

B. upon Mic19 depletion, the Sam50-Mic19-Mic60 axis was disrupted, and then the associated subunits Sam50, MTXs, Mic60, and Mic10 were degraded by the corresponding proteases, resulting in SAMICOS complex was interrupted and depolymerized. Although there is still the Sam50-Mic25-Mic60 axis, it is not enough to maintain the contact between mitochondrial inner- and outer- membranes. Therefore, as there is no 'blocking effect' of the SAMICOS complex, the CJs structure continues to shrink under the regulation of OPA1 and other factors and finally falls off from the inner membrane.

At the same time, the nascent cristae membrane continues produce in the absence of the SAMICOS super-complex, and the membrane fusion proceeds as that in WT cells, but cannot halt. Thus, the final cristae forms are the stacked closed membrane sheets lacking connection with the IBM (Harner et al., 2016b).

C. Expression of S-Mic19-Flag in Mic19 KO cells restores the MICOS complex, but without restoring Sam50, the Sam50-Mic19-Mic60 axis cannot be formed. Although, when we

simultaneously recover S-Mic19-Flag and exogenous Myc-sam50, the Sam50-Mic19-Mic60 axis still cannot be formed due to the defect of Mic19 N-terminal. Therefore, although all the elements, dimeric F1FO, OPA1, MICOS complex and SAM complex, are available, the CJ structure cannot be formed in the absence of interaction of SAM and MICOS complex.

D. Mic25, which is not affected in the absence of Mic19, could form a Sam50-Mic25-Mic60 axis with the 'residua' Sam50 and Mic60. However, this axis is not sufficient to maintain CJ due to loss of the dominant Sam50-Mic19-Mic60 axis. When Mic25 is overexpressed, plentiful Mic25 will recruit more Sam50 and Mic60 to generate more Sam50-Mic25-Mic60 axis. When a sufficient number of axes work together, it will reshape the SAMICOS super-complex. As a result, the inner mitochondrial membrane structure CJ can be reconstructed.

DISCUSSION

MICOS (mitochondrial contact site and cristae organizing system) complex is necessary for the formation of cristae organization and contact site between mitochondrial outer membrane and the inner boundary membrane. In the mammal, multiple subunits of MICOS complex were identified (Ott et al., 2015; van der Laan et al., 2016). However, how the contact between mitochondrial outer and inner membrane and crista structure are formed remain elusive. In this study, we report that Sam50-Mic19-Mic60 axis serves as a dominate 'bridge' to connect mitochondrial outer and inner membrane; moreover, Mic19 actually acts as a dominant bearing to link SAM and MICOS complex and form a supercomplex SAMICOS. SAMICOS regulates mitochondrial morphology and determines mitochondrial cristae architecture.

Mic19 can be cleaved at N-terminal by mitochondrial metalloprotease OMA1 when Mic19 detached from Sam50-Mic19-Mic60 axis either by depleting Sam50 or overexpressing Mic19. Why was little Mic19 cleaved under normal conditions (Figure 2C)? It is probably because the MICOS complex is assembled efficiently and precisely in proportion (Li et al., 2016), the expression of Mic19 is strictly regulated and there is no 'dissociative' Mic19; additionally, Sam50 bound to its N-terminus of Mic19 may make the cut site to be hidden. Thus, Mic19 cannot be cut under normal condition. However, the stresses, which cause Sam50 downregulation, should induce Mic19 cleavage.

In the last dozen years, MICOS and its subunits have been identified to be critical for mitochondrial membranes contact and cristae organization (Darshi et al., 2011; John et al., 2005). However, Mic60 or Mic19 deletion always accompanies with the disruption of whole

MICOS complex (Figures 1D and 6A). So it is hard to verify whether Mic60 or Mic19 alone is sufficient to regulate the cristae structure. Recently, Mic60 was reported to have the ability to bend liposomes in vitro (Hessenberger et al., 2017), making Mic60 being a dominant player in stabilizing and promoting cristae formation. In addition, in vitro assay also revealed that Mic10 oligomerization can efficiently bend liposomes (Barbot et al., 2015). These results suggest that Mic60 and Mic10 are cristae organization regulating effectors, and MICOS complex itself is supposed to be sufficient for cristae formation and organization. However, in our study, mitochondrial outer membrane protein Sam50, a core component of SAM complex (Kozjak et al., 2003), are severely involved in cristae organization. Sam50 knockdown led to abnormal cristae and disappearance of crista junctions, without affecting MICOS complex integrity and its core subunits Mic60 and Mic10 (Figure 5A), which gives us a hint that outer membrane SAM complex is also indispensable for crista junctions formation and we put forward a new viewpoint that Sam50 acted as an anchoring point in mitochondrial outer membrane for the structure of mitochondrial crista junctions (Figures 5E-5G). These data suggest that mitochondrial outer and inner membrane contact, linked by a supercomplex SAMICOS, play a critical role in cristae organization.

Mic19 depletion resulted in degradation of Sam50, Mic60, and Mic10, subsequently failed assembly of both MICOS and SAM complexes (Figures 1D-1G). The short form of Mic19 after cleavage (S-Mic19) maintained the ability to assemble and stabilize MICOS complex by interacting with Mic60, but failed to bind to Sam50 (Figure 3). The feather of S-Mic19 provides a good tool to study the role of individual MICOS complex in mitochondrial morphology and structure. Mic19 KO cells displayed abnormal mitochondrial morphology, loss of crista junctions and reduced ATP levels (Figures 4A-4F), S-Mic19 expression in Mic19 KO cells recovered MICOS complex, but failed to restore mitochondrial morphology, cristae structure and ATP production (Figures 4A-4F). Therefore, MICOS and SAM complexes cooperate together to form a supercomplex SAMICOS, which ensures mitochondrial outer and inner membrane contact and determine mitochondrial morphology and ultrastructure. Additionally, our identified SAMICOS complex is similar with MIB complex, a previous reported supercomplex (Ott et al., 2012), but the mechanism of MIB complex assembly and the role of MIB complex in mitochondrial morphology and structure are largely unknown.

Mic19 is highly conserved from yeast (Saccharomyces cerevisiae) to human. However, Mic25, an important paralog of Mic19, only exists in Metazoa (Rampelt et al., 2017), and the

role of Mic25 in the MICOS complex is still unclear since Mic25 depletion does not affect mitochondrial ultrastructure (Figures 6D, S4H, and S4I). In this study, we revealed that there is a functional overlap between Mic19 and Mic25. Mic19 possesses dominant position to form Sam50-Mic19-Mic60 axis, which directly links SAM and MICOS complex to form SAMICOS supercomplex for mediating mitochondrial outer and inner membrane contact. While Mic25 function as a back-up component, which can substitute for Mic19 to form Sam50-Mic25-Mic60 axis with the residual Sam50 and Mic60 when Mic19 is downregulated (Figures 6A-6C). Importantly, Mic19 could be cleaved by OMA1 under some stresses such as CCCP treatment, which results in disruption of Sam50-Mic19-Mic60 axis (Figures 3A-3D), but Mic25 could not be cleaved and remain stable (Figure 2H). Therefore, the Sam50-Mic25-Mic60 axis will protect the mitochondria to suffer some serious stresses. Mic19 plays a dominant role, whereas, Mic25 plays 'Emergency Protective' role when Mic19 was deleted. It is likely not only to be a more economical, but also a more secure mechanism for the survival of multicellular organisms.

Taken together, the main function of Mic19 or Mic25 is linking protein to connect and stabilize SAMICOS super-complex. The synergistic contact of mitochondrial outer and inner membrane mediated by SAMICOS is critical for the establishment and maintenance of mitochondrial cristae architecture.

CONFLICT OF INTEREST

The authors declare no conflict of interest.

ACKNOWLEDGEMENTS

We gratefully thank Dr. Jiahuai Han (Xiamen University) for the gift of cDNA colony, thank Dr. David Chan (California Institute of Technology) for communicating results before publication. This work is supported by National Natural Science Foundation of China (31471264 and 31671393), and the Fundamental Research Funds for the Central Universities (2042017kf0197 and 2042017kf0242).

MATERIALS AND METHODS

Cell culture, Antibodies and Reagents

All cell lines (MEFs, HeLa, HCT116 and 293T) were cultured in Dulbecco's Modified Eagle Medium (DMEM) supplemented with 10% (v/v) fetal bovine serum (PAN, Germany), 100 U/ml Penicillin and 100μg/ml Streptamycin (Gibco) and 1mM L-glutamine at 37℃ in 5% (v/v) CO2. Antibodies used in this study were: anti-Metaxin-2, anti-Prohibitin-2, anti-Mic60, anti-Yme1L, and anti-SDHA were purchased from Proteintech; anti-Mfn1, anti-Mfn2 and anti-Sam50 were from Abcam; anti-Metaxin-1, anti-Mic19 and anti-HSP60 were from Abclonal; anti-OMA1 was from Santa Cruz Biotechnology; anti-Mic10 was from Origene; anti-Drp1 and anti-OPA1 were purchased from BD Biosciences. Reagents used in this paper were: Carbonyl cyanide 3-chlorophenylhydrazone (CCCP, Sigma-Aldrich); Lipofectamine 2000 and Opti-MEM I (Invitrogen, Carlsbad, CA, USA) used for transient transfection with expression constructs according to the manufacturer's protocol.

Confocal Microscopy and Image Processing

Confocal images were collected using Leica microscope (Leica microsystem, Germany). All images for a given experiment were collected and adjusted in an identical manner. The Leica Application Suite software (Leica microsystem Corporation) was used for image processing and analysis. To determine mitochondrial morphology, cells were randomly selected for quantitative analysis and visually scored into five classifications ('Tubular', 'Short Tubular', 'Fragmented', 'Spherical- Expanded' and 'Large Spherical').

Electron Microscopy

The procedure for TEM was performed according to the previous report (McCaffery, 2007). the 100mM sodium cacodylate buffer were replaced by 100mM phosphate buffer without $CaCl_2$. The sections were supported on copper grids and then post-stained in uranyl acetate for 10min and then in lead citrate for 15 min, and the stained sections were imaged onto negatives using a JEOL electron microscope operated at 120 kV (JEM-1400 plus, Tokyo, Japan).

Statistical Methods

The data were presented as mean ± SD. Student's t-test was used to calculate P values. N.S. (non-significance); *P <0.05, **P < 0.01, and ***P<0.001.

REFERENCES

Alkhaja, A.K., Jans, D.C., Nikolov, M., Vukotic, M., Lytovchenko, O., Ludewig, F., Schliebs, W., Riedel, D., Urlaub, H., Jakobs, S., et al. (2012). MINOS1 is a conserved component of mitofilin complexes and required for mitochondrial function and cristae organization. Molecular biology of the cell *23*, 247-257.

An, J., Shi, J., He, Q., Lui, K., Liu, Y., Huang, Y., and Sheikh, M.S. (2012). CHCM1/CHCHD6, novel mitochondrial protein linked to regulation of mitofilin and mitochondrial cristae morphology. The Journal of biological chemistry *287*, 7411-7426.

Baker, M.J., Lampe, P.A., Stojanovski, D., Korwitz, A., Anand, R., Tatsuta, T., and Langer, T. (2014). Stress-induced OMA1 activation and autocatalytic turnover regulate OPA1-dependent mitochondrial dynamics. The EMBO journal *33*, 578-593.

Barbot, M., Jans, D.C., Schulz, C., Denkert, N., Kroppen, B., Hoppert, M., Jakobs, S., and Meinecke, M. (2015). Mic10 oligomerizes to bend mitochondrial inner membranes at cristae junctions. Cell metabolism *21*, 756-763.

Barrera, M., Koob, S., Dikov, D., Vogel, F., and Reichert, A.S. (2016). OPA1 functionally interacts with MIC60 but is dispensable for crista junction formation. FEBS letters *590*, 3309-3322.

Bohnert, M., Zerbes, R.M., Davies, K.M., Muhleip, A.W., Rampelt, H., Horvath, S.E., Boenke, T., Kram, A., Perschil, I., Veenhuis, M., et al. (2015). Central role of Mic10 in the mitochondrial contact site and cristae organizing system. Cell metabolism *21*, 747-755.

Capala, M.E., Pruis, M., Vellenga, E., and Schuringa, J.J. (2016). Depletion of SAM50 Specifically Targets BCR-ABL-Expressing Leukemic Stem and Progenitor Cells by Interfering with Mitochondrial Functions. Stem cells and development *25*, 427-437.

Cho, B., Cho, H.M., Jo, Y., Kim, H.D., Song, M., Moon, C., Kim, H., Kim, K., Sesaki, H., Rhyu, I.J., et al. (2017). Constriction of the mitochondrial inner compartment is a priming event for mitochondrial division. Nature communications *8*, 15754.

Darshi, M., Mendiola, V.L., Mackey, M.R., Murphy, A.N., Koller, A., Perkins, G.A., Ellisman, M.H., and Taylor, S.S. (2011). ChChd3, an inner mitochondrial membrane protein, is essential for maintaining crista integrity and mitochondrial function. The Journal of biological chemistry *286*, 2918-2932.

Darshi, M., Trinh, K.N., Murphy, A.N., and Taylor, S.S. (2012). Targeting and import mechanism of coiled-coil helix coiled-coil helix domain-containing protein 3 (ChChd3) into the mitochondrial intermembrane space. The Journal of biological chemistry *287*, 39480-39491.

Davies, K.M., Anselmi, C., Wittig, I., Faraldo-Gomez, J.D., and Kuhlbrandt, W. (2012). Structure of the yeast F1Fo-ATP synthase dimer and its role in shaping the mitochondrial cristae. eLife *109*, 13602-13607.

Demongeot, J., Glade, N., Hansen, O., and Moreira, A. (2007). An open issue: the inner mitochondrial membrane (IMM) as a free boundary problem. Biochimie *89*, 1049-1057.

Genin, E.C., Plutino, M., Bannwarth, S., Villa, E., Cisneros-Barroso, E., Roy, M., Ortega-Vila, B., Fragaki, K., Lespinasse, F., Pinero-Martos, E., et al. (2016). CHCHD10 mutations promote loss of mitochondrial cristae junctions with impaired mitochondrial genome maintenance and inhibition of apoptosis. EMBO molecular medicine *8*, 58-72.

Guarani, V., McNeill, E.M., Paulo, J.A., Huttlin, E.L., Frohlich, F., Gygi, S.P., Van Vactor, D., and Harper, J.W. (2015). QIL1 is a novel mitochondrial protein required for MICOS complex stability and cristae morphology. eLife *4*.

Harner, M., Korner, C., Walther, D., Mokranjac, D., Kaesmacher, J., Welsch, U., Griffith, J., Mann, M., Reggiori, F., and Neupert, W. (2011). The mitochondrial contact site complex, a determinant of mitochondrial architecture. The EMBO journal *30*, 4356-4370.

Harner, M.E., Unger, A.K., Geerts, W.J., Mari, M., Izawa, T., Stenger, M., Geimer, S., Reggiori, F., and Westermann, B. (2016a). An evidence based hypothesis on the existence of two pathways of mitochondrial crista formation.

5.

Harner, M.E., Unger, A.K., Geerts, W.J., Mari, M., Izawa, T., Stenger, M., Geimer, S., Reggiori, F., Westermann, B., and Neupert, W. (2016b). An evidence based hypothesis on the existence of two pathways of mitochondrial crista formation. eLife *5*.

Hering, T., Kojer, K., Birth, N., Hallitsch, J., Taanman, J.W., and Orth, M. (2017). Mitochondrial cristae remodelling is associated with disrupted OPA1 oligomerisation in the Huntington's disease R6/2 fragment model. Experimental neurology *288*, 167-175.

Hessenberger, M., Zerbes, R.M., Rampelt, H., Kunz, S., Xavier, A.H., Purfurst, B., Lilie, H., Pfanner, N., van der Laan, M., and Daumke, O. (2017). Regulated membrane remodeling by Mic60 controls formation of mitochondrial crista junctions. Nature communications *8*, 15258.

Hohr, A.I., Straub, S.P., Warscheid, B., Becker, T., and Wiedemann, N. (2015). Assembly of beta-barrel proteins in the mitochondrial outer membrane. Biochimica et biophysica acta *1853*, 74-88.

Hoppins, S., Collins, S.R., Cassidy-Stone, A., Hummel, E., Devay, R.M., Lackner, L.L., Westermann, B., Schuldiner, M., Weissman, J.S., and Nunnari, J. (2011). A mitochondrial-focused genetic interaction map reveals a scaffold-like complex required for inner membrane organization in mitochondria. The Journal of cell biology *195*, 323-340.

Huynen, M.A., Muhlmeister, M., Gotthardt, K., Guerrero-Castillo, S., and Brandt, U. (2016). Evolution and structural organization of the mitochondrial contact site (MICOS) complex and the mitochondrial intermembrane space bridging (MIB) complex. Biochimica et biophysica acta *1863*, 91-101.

Jian, F., Chen, D., Chen, L., Yan, C., Lu, B., Zhu, Y., Chen, S., Shi, A., Chan, D.C., and Song, Z. (2018). Sam50 Regulates PINK1-Parkin-Mediated Mitophagy by Controlling PINK1 Stability and Mitochondrial Morphology. Cell reports *23*, 2989-3005.

John, G.B., Shang, Y., Li, L., Renken, C., Mannella, C.A., Selker, J.M., Rangell, L., Bennett, M.J., and Zha, J. (2005). The mitochondrial inner membrane protein mitofilin controls cristae morphology. Molecular biology of the cell *16*, 1543-1554.

Koob, S., Barrera, M., Anand, R., and Reichert, A.S. (2015). The non-glycosylated isoform of MIC26 is a constituent of the mammalian MICOS complex and promotes formation of crista junctions. Biochimica et biophysica acta *1853*, 1551-1563.

Kozjak, V., Wiedemann, N., Milenkovic, D., Lohaus, C., Meyer, H.E., Guiard, B., Meisinger, C., and Pfanner, N. (2003). An essential role of Sam50 in the protein sorting and assembly machinery of the mitochondrial outer membrane. The Journal of biological chemistry *278*, 48520-48523.

Li, H., Ruan, Y., Zhang, K., Jian, F., Hu, C., Miao, L., Gong, L., Sun, L., Zhang, X., Chen, S., et al. (2016). Mic60/Mitofilin determines MICOS assembly essential for mitochondrial dynamics and mtDNA nucleoid organization. Cell death and differentiation *23*, 380-392.

Mannella, C.A. (2006). Structure and dynamics of the mitochondrial inner membrane cristae. Biochimica et biophysica acta *1763*, 542-548.

McCaffery, E.M.P.a.J.M. (2007). Conventional and immunoelectron microscopy of mitochondria. Methods in Molecular Biology *372*.

Merkwirth, C., Dargazanli, S., Tatsuta, T., Geimer, S., Lower, B., Wunderlich, F.T., von Kleist-Retzow, J.C., Waisman, A., Westermann, B., and Langer, T. (2008). Prohibitins control cell proliferation and apoptosis by regulating OPA1-dependent cristae morphogenesis in mitochondria. Genes & development *22*, 476-488.

Ott, C., Dorsch, E., Fraunholz, M., Straub, S., and Kozjak-Pavlovic, V. (2015). Detailed analysis of the human mitochondrial contact site complex indicate a hierarchy of subunits. PloS one *10*, e0120213.

Ott, C., Ross, K., Straub, S., Thiede, B., Gotz, M., Goosmann, C., Krischke, M., Mueller, M.J., Krohne, G., Rudel, T., et al. (2012). Sam50 functions in mitochondrial intermembrane space bridging and biogenesis of respiratory

complexes. Molecular and cellular biology *32*, 1173-1188.

Pfanner, N., van der Laan, M., Amati, P., Capaldi, R.A., Caudy, A.A., Chacinska, A., Darshi, M., Deckers, M., Hoppins, S., Icho, T., et al. (2014). Uniform nomenclature for the mitochondrial contact site and cristae organizing system. The Journal of cell biology *204*, 1083-1086.

Quiros, P.M., Ramsay, A.J., and Lopez-Otin, C. (2013). New roles for OMA1 metalloprotease: From mitochondrial proteostasis to metabolic homeostasis. Adipocyte *2*, 7-11.

Rabl, R., Soubannier, V., Scholz, R., Vogel, F., Mendl, N., Vasiljev-Neumeyer, A., Korner, C., Jagasia, R., Keil, T., Baumeister, W., et al. (2009). Formation of cristae and crista junctions in mitochondria depends on antagonism between Fcj1 and Su e/g. The Journal of cell biology *185*, 1047-1063.

Rampelt, H., Zerbes, R.M., van der Laan, M., and Pfanner, N. (2017). Role of the mitochondrial contact site and cristae organizing system in membrane architecture and dynamics. Biochimica et biophysica acta *1864*, 737-746.

Ruan, Y., Li, H., Zhang, K., Jian, F., Tang, J., and Song, Z. (2013). Loss of Yme1L perturbates mitochondrial dynamics. Cell death & disease *4*, e896.

Sastri, M., Darshi, M., Mackey, M., Ramachandra, R., Ju, S., Phan, S., Adams, S., Stein, K., Douglas, C.R., Kim, J.J., et al. (2017). Sub-mitochondrial localization of the genetic-tagged mitochondrial intermembrane space-bridging components Mic19, Mic60 and Sam50. Journal of cell science *130*, 3248-3260.

Semenzato, M., Cogliati, S., and Scorrano, L. (2011). Prohibitin(g) cancer: aurilide and killing by Opa1-dependent cristae remodeling. Chemistry & biology *18*, 8-9.

van der Laan, M., Bohnert, M., Wiedemann, N., and Pfanner, N. (2012). Role of MINOS in mitochondrial membrane architecture and biogenesis. Trends in cell biology *22*, 185-192.

van der Laan, M., Horvath, S.E., and Pfanner, N. (2016). Mitochondrial contact site and cristae organizing system. Current opinion in cell biology *41*, 33-42.

Weber, T.A., Koob, S., Heide, H., Wittig, I., Head, B., van der Bliek, A., Brandt, U., Mittelbronn, M., and Reichert, A.S. (2013). APOOL is a cardiolipin-binding constituent of the Mitofilin/MINOS protein complex determining cristae morphology in mammalian mitochondria. PloS one *8*, e63683.

Wenz, L.S., Opalinski, L., Schuler, M.H., Ellenrieder, L., Ieva, R., Bottinger, L., Qiu, J., van der Laan, M., Wiedemann, N., Guiard, B., et al. (2014). The presequence pathway is involved in protein sorting to the mitochondrial outer membrane. EMBO reports *15*, 678-685.

Zerbes, R.M., van der Klei, I.J., Veenhuis, M., Pfanner, N., van der Laan, M., and Bohnert, M. (2012). Mitofilin complexes: conserved organizers of mitochondrial membrane architecture. Biological chemistry *393*, 1247-1261.

Zhang, K., Li, H., and Song, Z. (2014). Membrane depolarization activates the mitochondrial protease OMA1 by stimulating self-cleavage. EMBO reports *15*, 576-585.

Zick, M., Rabl, R., and Reichert, A.S. (2009). Cristae formation-linking ultrastructure and function of mitochondria. Biochimica et biophysica acta *1793*, 5-19.

FIGURE LEGENDS

Figure 1. Mic19 stabilizes SAM and MICOS complexes and bridges SAM and MICOS to form a supercomplex SAMICOS.

(A) Myc-Sam50 and Mic19-Flag were transiently co-expressed in 293T cells and co-immunoprecipitation (Co-IP) assay were performed with anti-Flag M2 resin. The eluted protein samples were detected by Western blot analysis.

(B-C) GST pull-down experiments were performed by using Pierce Glutathione Agarose and Western blot analysis using antibodies against GST or His to demonstrate the interaction between Mic19 and Sam50 or Mic19 and Mic60 (371-590).

(D) Protein levels of wild-type cells (control), Mic19 knockout (Mic19 KO) HeLa cells were analyzed by SDS-PAGE and immunoblotting using indicated antibodies, and Tubulin was used as loading control.

(E) Mic19-Flag was recovered exogenously in Mic19 KO HeLa cells, and lysates were analyzed by western blot with indicated antibodies, and Tubulin was served as loading control.

(F-G) Mic19 knockout leads to de-polymerization of SAM complex and MICOS complex. Mitochondrial protein samples from HeLa WT cells, Mic19 KO cells and Mic19 knockout recovering Mic19-Flag cells (F) or protein samples from WT and cardiac-specific Mic19 KO mice (G). All the protein samples were subjected to BN-PAGE, and the related complexes were analyzed by western blot analysis with antibody against Mic19, Mic60 and Sam50 respectively. The bands of the complexes are labeled with corresponding boxes. The SAMICOS complex is approximately 2000kDa and the MICOS is approximately 700kDa. The complex, approximately 250kDa, is SAM complexes and ~125kDa is unidentified complex containing Sam50 accordingly. SDHA, identifying the size of complex II, served as loading control.

Figure 2. Mic19 detached from SAMICOS complexes can be cleaved at N-terminal by mitochondrial protease OMA1

(A) Loss of Sam50 (shSam50 7.5days) in WT or Yme1L KO HCT116 cells respectively, and lysates were analyzed by Western blotting. GAPDH was used as loading control.

(B) Sam50 was down-regulated (shSam50 7.5days) in WT or OMA1 KO HCT116 cells respectively. Western blotting analysis was performed using the indicated antibody.

(C) HeLa cells stably expressing human Mic19-Flag were treated with DMSO or CCCP (20μM, 4 h), and the cell lysates were analyzed by Western blot using Mic19 or Flag antibodies.

(D) WT or OMA1 KO MEFs cells expressing Mic19-Flag were treated with DMSO or CCCP (20μM, 4 h). Western blotting analysis was performed to examine the Mic19-Flag cleavage, and HSP60 or GAPDH used as loading control.

(E) OMA1^{E324Q}-Flag transiently transfect into 293T cells. Co-IP was performed using anti-Flag M2 resin and the eluted protein samples were analyzed by Western blotting to detect the interaction between OMA1 and Mic19.

(F) The schematic presentation of human Mic19 and Mic25 domain. 'DUF737' indicates domain of unknown function; 'CHCH' indicates coiled-coil helix-coiled-coil helix domain. The right showed the comparison of Mic19 N-terminal 26-39AA and Mic25 N-terminal 28-41AA.

(G) HeLa cells expressing Mic19-Flag and indicated Mic19 mutation constructs (Flag-tagged) were treated with DMSO or CCCP (20μM, 4 h) and the cell lysates were analyzed by Western blot using Flag antibodies. "Δ" indicates deletion of residues.

(H-J) HeLa cells expressing Mic25-Flag (H) or indicated Mic25 mutation constructs (I), HCT116 WT or OMA1 KO cells expressing Mic25 mutation constructs (J) were treated with DMSO or CCCP (20μM, 4 h). Western blot was performed using indicated antibodies.

Figure 3. Interaction between Mic19 and Sam50 is required for the integrity of SAMICOS complex

(A) Mic19-Flag, S-Mic19-Flag, and Mic19 (1-35aa)-Flag were transiently transfected into 293T cells, and then co-immunoprecipitation (Co-IP) assay with anti-Flag M2 resin and Western blotting analysis were performed to examine the interactions.

(B, C, D) GST pull-down assay were performed by using Pierce Glutathione Agarose and Western blot analysis using antibodies against GST or His to demonstrate the interactions. (B) The examination of direct interaction between Mic19 (1-35AA) and Sam50. (C) The demonstration of direct interaction between S-Mic19 and Sam50. (D) The detection of direct interaction between Mic19 (1-35AA) or S-Mic19 with Mic60 (371-590).

(E) Mitochondria were extracted from WT, Mic19 KO, Mic19$^{\Delta gRNA}$-Flag, or S-Mic19$^{\Delta gRNA}$-Flag HeLa cells, then non-denatured protein samples from mitochondria were analyzed by BN-PAGE and Western blotting. The bands of the complexes are labeled with corresponding boxes.

(F) Mic19$^{\Delta gRNA}$-Flag, S-Mic19$^{\Delta gRNA}$-Flag, and Mic19 $^{(ID33\text{-}34VN)\Delta gRNA}$-Flag were stably expressed in Mic19 KO HeLa cells respectively. Cell lysates were analyzed by Western blot using indicated antibodies.

Figure 4. SAMICOS complex is critical for the maintenance of normal mitochondrial morphology and mitochondrial crista junctions.

(A) Mic19 KO HeLa cells expressing Mic19$^{\Delta gRNA}$-Flag, S-Mic19$^{\Delta gRNA}$-Flag and Mic19 $^{(ID33-34VN)\Delta gRNA}$-Flag respectively, and mitochondrial morphology of all cell lines expressing mito-GFP was visualized by confocal microscope.

(B) Statistical analysis was performed according to the criteria detailed in "Materials and Methods". Error bars indicate the mean ±SD of three independent experiments in which 100 cells were scored, ***P<0.001.

(C) S-Mic19 cannot restore CJs structure even if the MICOS complex was reconstructed. Mitochondrial crista junctions structure in WT, Mic19 KO, Mic19 KO_Mic19-Flag, Mic19 KO_S-Mic19-Flag, Mic19 KO_Myc-Sam50, or Mic19 KO_S-Mic19-Flag_Myc-Sam50 HeLa cells were analyzed by transmission electron microscope (TEM). The ultrathin section sample was observed using an electron microscope (JEM-1400plus, Tokyo, Japan) under the condition of an accelerating voltage of 120 kV.

(D) Statistics of the mitochondrial ultrastructure of all related cell lines. The mean value and standard deviations (S.D.) were calculated from 3 independent experiments in which 100 mitochondrial cristae and the number of corresponding CJs were counted. Error bars represent means ± SD of three independent experiments, ***P<0.001 vs WT.

(E) BN-PAGE and Western blot analysis for the related cell lines were performed to examine the assembly of complex. The bands of the complexes are labeled with corresponding boxes. The SAMICOS complex is approximately 2000kDa, and the MICOS is approximately 700kDa. The complex, approximately 250kDa, is SAM complexes, and ~125kDa is unidentified complex containing Sam50 accordingly. SDHA, identifying the size of complex II, served as loading control.

(F) The relative ATP level of WT, Mic19 KO, Mic19 KO_Mic19-Flag, Mic19 KO_S-Mic19-Flag, Mic19 KO_Myc-Sam50, or Mic19 KO_S-Mic19-Flag_Myc-Sam50 HeLa cells were measured using an ATP assay kit. Error bars represent means ± SD of three independent experiments, ***P<0.001 vs WT.

Figure 5. Sam50 acting as an anchoring point in outer membrane is required for the formation of mitochondrial crista junctions.

(A) Down-regulate Sam50 (shSam50 for 5days) in WT, Mic19KO_Mic19$^{\Delta gRNA}$-Flag, or

Mic19KO_Mic19 $^{(ID33\text{-}34VN)\Delta gRNA}$-Flag expressed HeLa cells, and protein levels of the related cells were analyzed by Western blotting. Tubulin was used as loading control.

(B) The mitochondrial morphology of WT, Mic19KO_Mic19$^{\Delta gRNA}$-Flag, or Mic19KO_Mic19 $^{(ID33\text{-}34VN)\Delta gRNA}$-Flag expressed HeLa cells with or without Sam50 knockdown were analyzed by confocal microscope. Anti-HSP60 was used for immunofluorescence to show mitochondrial morphology.

(C) Mitochondrial morphology was classified into three types (tubular, short tubular and fragmented) and calculated using statistical software. Bars represent means ±S.D. of three independent experiments.

(D-E) The mitochondrial cristae junction structure of WT, Mic19KO_Mic19$^{\Delta gRNA}$-Flag cells, and Mic19KO_Mic19 (ID33-34VN$^{)\Delta gRNA}$-Flag HeLa cells with or without Sam50 knockdown were analyzed by transmission electron microscope (TEM).

(F) Statistics of the mitochondrial ultrastructure of all related cell lines. The mean value and standard deviations (S.D.) were calculated from 3 independent experiments in which 100 mitochondrial cristae and the number of corresponding CJs were counted, ***P<0.001.

(G) Sam50 is likely to be located in the CJs structure. Flag-Sam50 was stably expressed in COS7 cells and MitoTracker® Red CMXRos dye was used to label mitochondria. Immunofluorescence staining was performed with Flag antibody, and imaging obtained by STED, a super-resolution microscope. The right side is a schematic diagram for Flag-Sam50 location.

(H) Statistical analysis of all Flag-Sam50 dots on the outer membrane mitochondria and the corresponding position against to the CJs structure.

Figure 6. Restoration of Sam50-X-Mic60 axis by overexpressed Mic25 in Mic19 KO cells can also reconstruct the mitochondrial crista junctions.

(A) The indicated Protein levels of MEF WT cells, shMic60 cells, Mic19 KO cells, or Mic19 KO plus shMic60 cells were analyzed by Western blotting.

(B) Myc-Sam50 and Mic25-Flag were transiently co-expressed in 293T cells and co-immunoprecipitation (Co-IP) assay were performed with anti-Flag M2 resin. The eluted protein samples were detected by Western blot analysis.

(C) GST pull-down experiments were performed by using Pierce Glutathione Agarose and Western blot analysis using antibodies against GST or His to demonstrate the interaction

between Mic25 and Sam50 or Mic60.

(D-F) WT (D), Mic19 KO (E), or Mic25 KO (F) HeLa cells expressing mito-GFP respectively were knocked down for Mic19 (shMic19) or Mic25 (shMic25), and mitochondrial morphology was analyzed by confocal microscope.

(G) Mitochondrial morphology in all cell lines shown in "D-F" were classified and counted according to the criteria detailed in Materials and Methods, and bars represent means ±S.D. of three independent experiments, ***P<0.001.

(H) Mic25-Flag was stably overexpressed in Mic19 KO cells expressing mito-GFP, and immunofluorescence staining was performed with Flag antibody. Mitochondrial morphology was analyzed by confocal microscope.

(I) Statistical analysis was performed according to the criteria detailed in "Materials and Methods", the mean value and standard deviations (S.D.) were calculated from 3 independent experiments in which 100 cells were scored, ***P<0.001.

(J) For all cell lines shown in "Figure H", protein samples were prepared, and Western blotting analysis was performed using the corresponding antibodies.

(K) The mitochondrial cristae junction structure of WT, Mic19 KO, or Mic25 overexpressed Mic19 KO HeLa cells were analyzed by transmission electron microscope (TEM).

(L) Statistics of the mitochondrial ultrastructure of all cell lines shown in figure H. The mean value and standard deviations (S.D.) were calculated from 3 independent experiments in which 100 mitochondrial cristae and the number of corresponding CJs were counted, ***P<0.001.

(M) The relative ATP level of WT, Mic19 KO, or Mic25 overexpressed Mic19 KO HeLa cells were measured using an ATP assay kit. Error bars represent means ± SD of three independent experiments, ***P<0.001 vs WT.

Figure 7. Theoretical model of SAM-MICOS complex functions on the formation of the CJs structure.

In this schematic, the mitochondrial outer membranes and inner membrane form an arc. In the arc, we simulated the formation of mitochondrial cristae and CJ structures. In the inside of the arc, the large arrow represents the direction of the formation or disappearance for mitochondrial cristae and CJ structures. If the tail of the large arrow changes from 'thin' to 'thick', it indicates the formation process. If the tail of the large arrow changes from 'thick' to 'thin', it indicates the disappearance process. In the innermost of the arc, simulated mitochondria represent the

final mitochondrial cristae and CJs structure in each model【CJs, cristae junction site; Blue lines, the mitochondrial outer membrane (OM); Red lines, the mitochondrial inner boundary membrane (IBM) and cristae membrane (CM)】.

SUPPLEMENTAL FIGURE LEGENDS

Figure S1 (Related to Figure 1).

(A) GST pull-down assay were performed to demonstrate the interaction between Mic19 and Mic25.

(B) Lysates from control or Mic25 knockout (Mic25 KO) HeLa cells were analyzed by Western blot with antibodies against the indicated proteins, and Tubulin was served as loading control.

(C) Equal protein samples from control, Mic10 knockout (Mic10 KO) HeLa cells were separated by SDS-PAGE, and Western blot analysis was preformed to detect the related protein.

(D) Lysates of control or shSam50 HeLa cells were analyzed by Western blotting using indicated antibodies. Tubulin assayed as protein-loading control.

(E) Mouse liver lysates of liver-specific Mic19 KO mice were analyzed by BN-PAGE and Western blotting. The bands of the complexes are labeled with corresponding boxes. The SAMICOS complex is approximately 2000kDa and the MICOS is approximately 700kDa. The complex, approximately 250kDa, is SAM complexes and ~125kDa is unidentified complex containing Sam50 accordingly. SDHA, identifying the size of complex II, served as loading control.

Figure S2 (Related to Figure 2).

(A) Sam50 degradation, caused by deletion of Mic19, is related to Yme1L. Down-regulation of Mic19 in WT, shYme1L MEFs cells respectively, and lysates were analyzed by Western blotting.

(B) Flag-Sam50 was transiently transfected into 293T cells, and Co-IP was performed using anti-Flag M2 resin and Western blotting was performed to detect the interaction between Sam50 and Yme1L.

(C-D) Depletion of Mic60 (shMic60 5days) in MEFs cells or knockout of Mic25 in HeLa cells, lysates were analyzed by Western blotting to examine the cleavage of Mic19 or other subunit, and Tubulin or GAPDH was served as loading control.

(E) Mic19-Flag was transiently transfected into 293T cells, and lysates were analyzed by Western blotting using Mic19 or Flag antibody.

(F) OMA1 KO HCT116 cells expressing Mic19-Flag were treated with DMSO or CCCP (20μM, 4 h). Western blot was performed to detect the cleavage.

(G) The protein amino acid sequences of Mic19 multiple species and human Mic25 were obtained on NCBI, and then analyzed using sequence alignment software DNAMAN.

(H) Mic19-Flag&OMA1^{E324Q}-Myc or Mic19$^{ID33\text{-}34VN}$-Flag&OMA1^{E324Q}-Myc were co-expressed in 293T cells. Co-immunoprecipitation assay and Western blotting was performed to examine the interactions.

Figure S3 (Related to Figure 4).

(A) Myc-Sam50 were stably expressing in S-Mic19$^{\Delta gRNA}$-Flag cells by infecting Myc-Sam50 retrovirus. 72 hours after infection, the cell lysates were analyzed by Western blot using indicated antibodies to detect the related subunits.

(B) S-Mic19ΔgRNA-Flag and Myc-Sam50 were co-expressed in the Mic19 KO HeLa cell line. Mitochondrial morphology of all cell lines expressing mito-GFP was visualized by confocal microscope.

(C) Statistical analysis was performed according to the criteria detailed in Materials and Methods; the mean value and standard deviations (S.D.) were calculated from 3 independent experiments in which 100 cells were scored, ***P<0.001.

Figure S4 (Related to Figure 6).

(A, B) WT or Mic19 KO MEFs cells were knocked down for Mic60 respectively, and mitochondria were labeled by immunostaining using anti-HSP60 antibody, mitochondrial morphology were analyzed by confocal microscope, and statistical analysis was performed according to the criteria detailed in “Materials and Methods”; the mean value and standard deviations (S.D.) were calculated from 3 independent experiments in which 100 cells were scored.

(C) Protein levels of all related cell lines were examined by western blotting using the indicated antibodies. Tubulin protein was used as loading control.

(D-E) Lysates from HeLa cells expressing Mic19-Flag or Mic25-Flag (D) and the diluted protein lysates (E) were analyzed by western blot analysis with indicated antibodies.

(F-G) Densitometry analysis was performed using ImageJ software to calculate the relative expression levels of endogenous Mic19 and Mic25 in HeLa cells. The relative expression of

Mic19 is set to 1, the expression of Mic25 is calculated according to the formulation in “F”, the data is shown in “G”.

(H) The mitochondrial cristae junction structure of WT, Mic25 KO were analyzed by transmission electron microscope (TEM).

(I) Statistics of the mitochondrial ultrastructure of WT and Mic25 KO cell lines. The mean value and standard deviations (S.D.) were calculated from 3 independent experiments in which 100 mitochondrial cristae and the number of corresponding CJs were counted.

SUPPLEMENTAL EXPERIMENTAL TABLE

Table S1. Selected Tandem mass spectrometry (MS/MS) data from the eluted protein samples of Mic19-Flag Co-IP assay.

Gene Name	Description	MW (kDa)	Σ# Unique Peptides	Σ# PSMs
MIC60/IMMT	Mitochondrial inner membrane protein	83.63	61	255
MIC19/CHCHD3	Coiled-coil-helix-coiled-coil-helix domain-containing protein 3	26.14	22	314
MTX2	Metaxin-2	29.74	13	38
SLC25A5	ADP/ATP translocase 2	32.87	5	18
MIC25/CHCHD6	Coiled-coil-helix-coiled-coil-helix domain-containing protein 6	26.44	8	12
SAM50	Sorting and assembly machinery component 50 homolog	51.94	16	65
HSP1A	Heat shock 70kDa protein 1A/1B	70.01	20	64
HSPD1	60kDa heat shock protein, mitochondrial	61.02	10	18
PGAM5	Serine/threonine-protein phosphatase PGAM5	31.98	4	8
ATP5C1	ATP synthase subunit gamma, mitochondrial	32.98	5	10
ATP5B	ATP synthase subunit beta, mitochondrial	56.52	7	13
COX2	Cytochrome c oxidase subunit 2	25.55	2	4
UQCRC2	Cytochrome b-c1 complex subunit 2, mitochondrial	48.41	4	7

Table S1. Selected Tandem mass spectrometry (MS/MS) data. Mic19-Flag was transiently expressed in 293T cells, and co-immunoprecipitation (Co-IP) assay was performed with anti-Flag M2 resin. The eluted protein samples were analyzed by MS/MS and the indicated proteins from MS/MS data was displayed in this table. The indicated protein of molecular weight (MW), the number and of total peptide spectrum matching (PSMs), the number of total unique peptides (Coverage) identified by MS are shown.

Figure 1

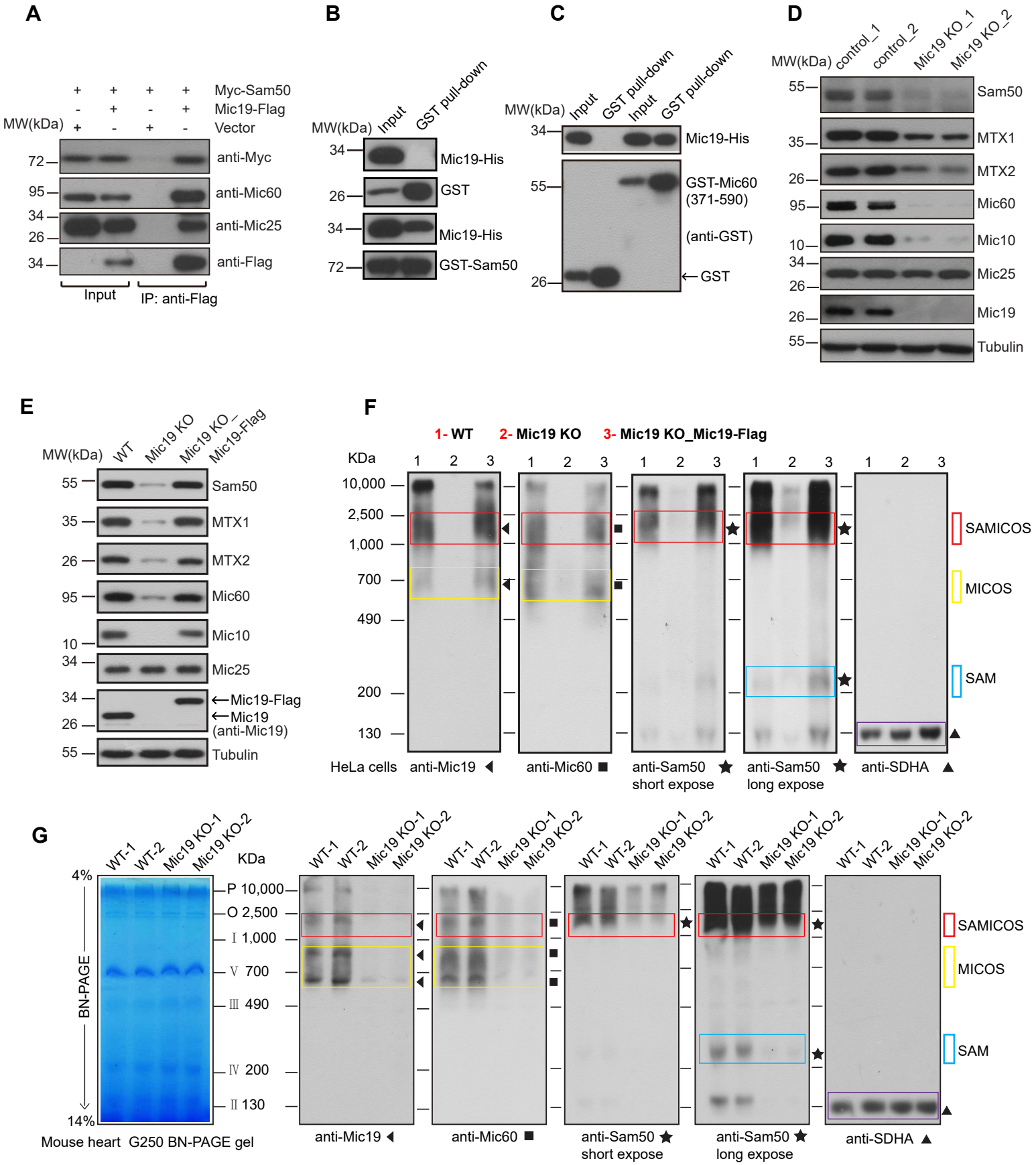

Figure 2

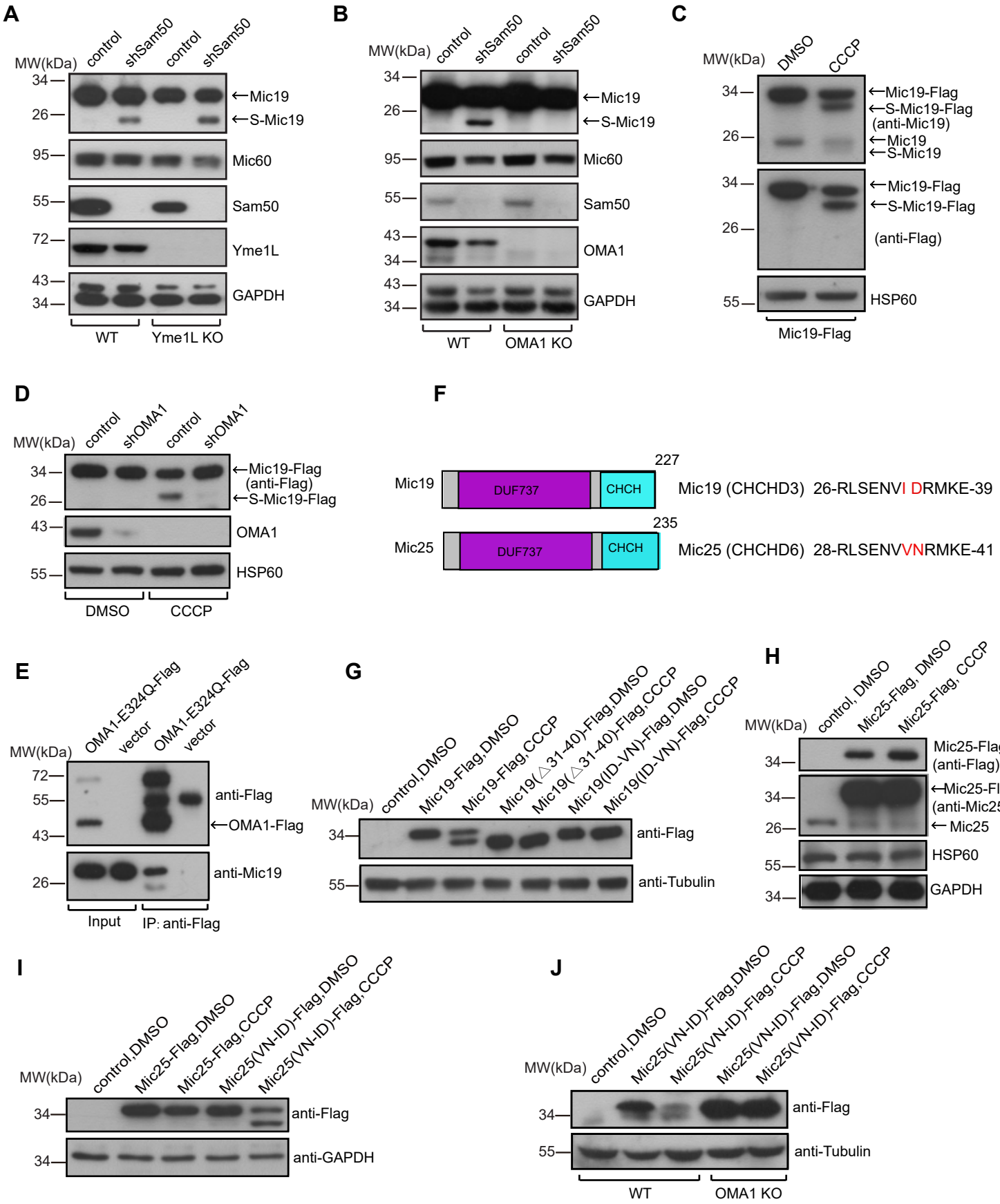

Figure 3

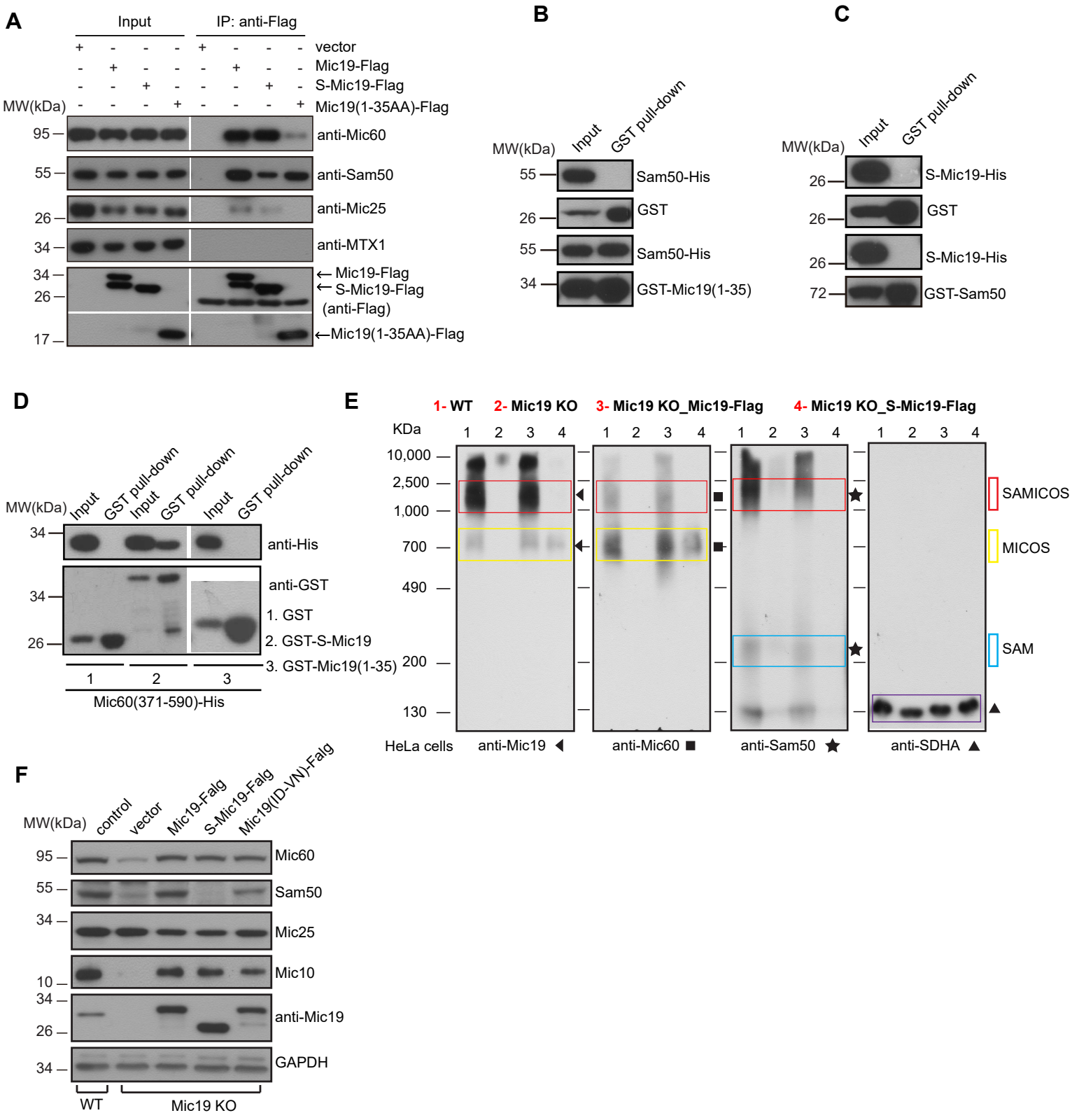

Figure 4

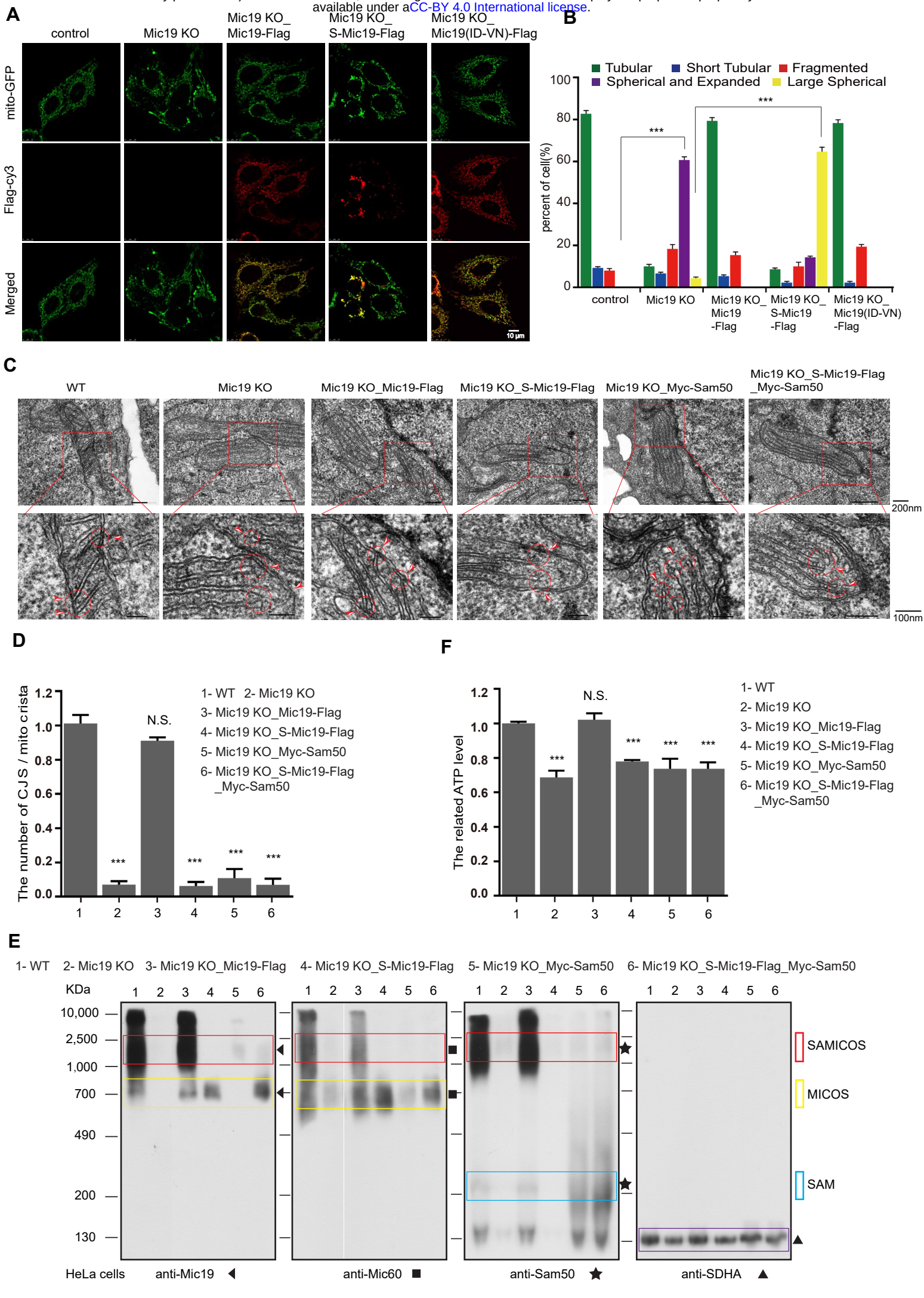

Figure 5

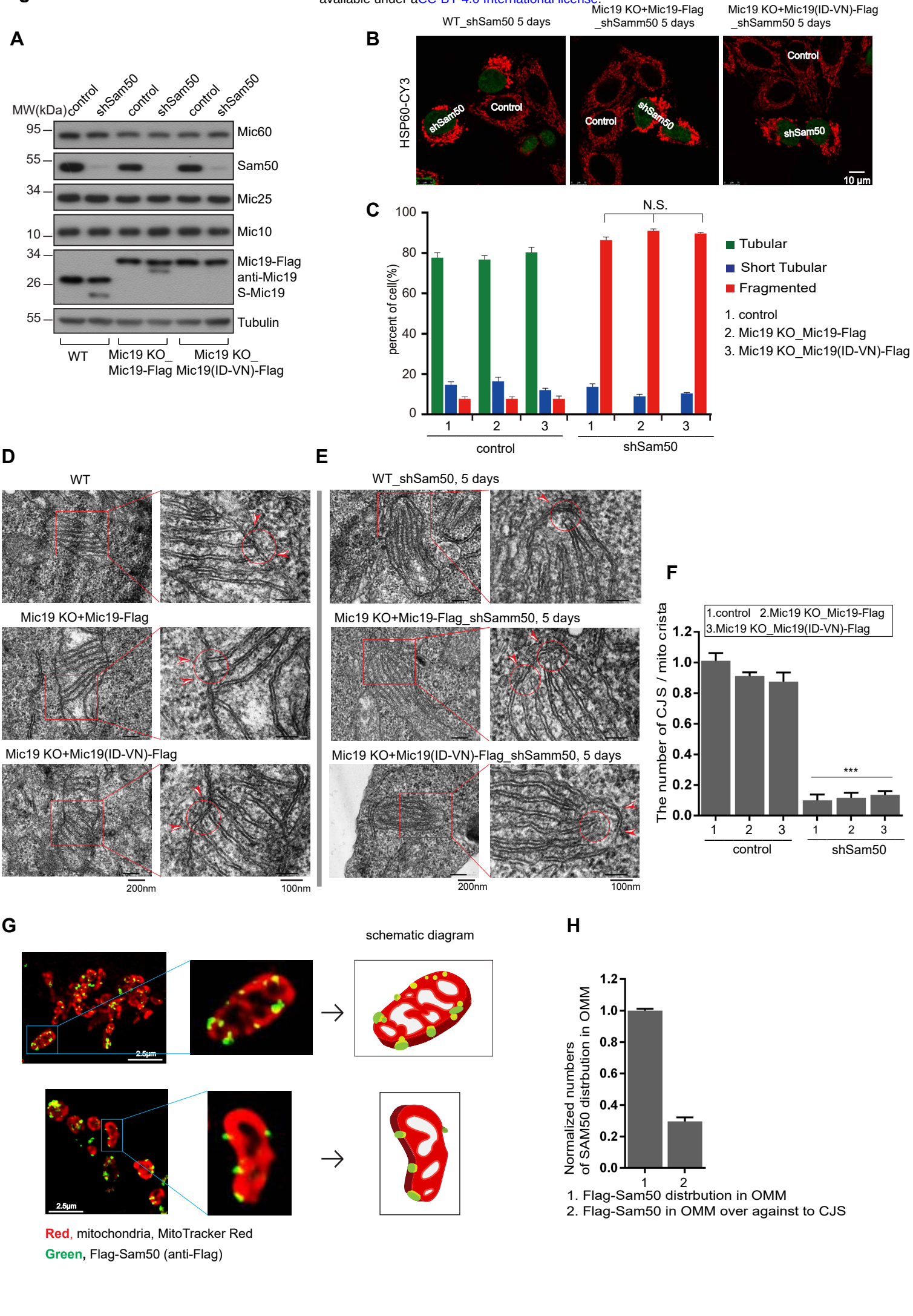

Figure 6

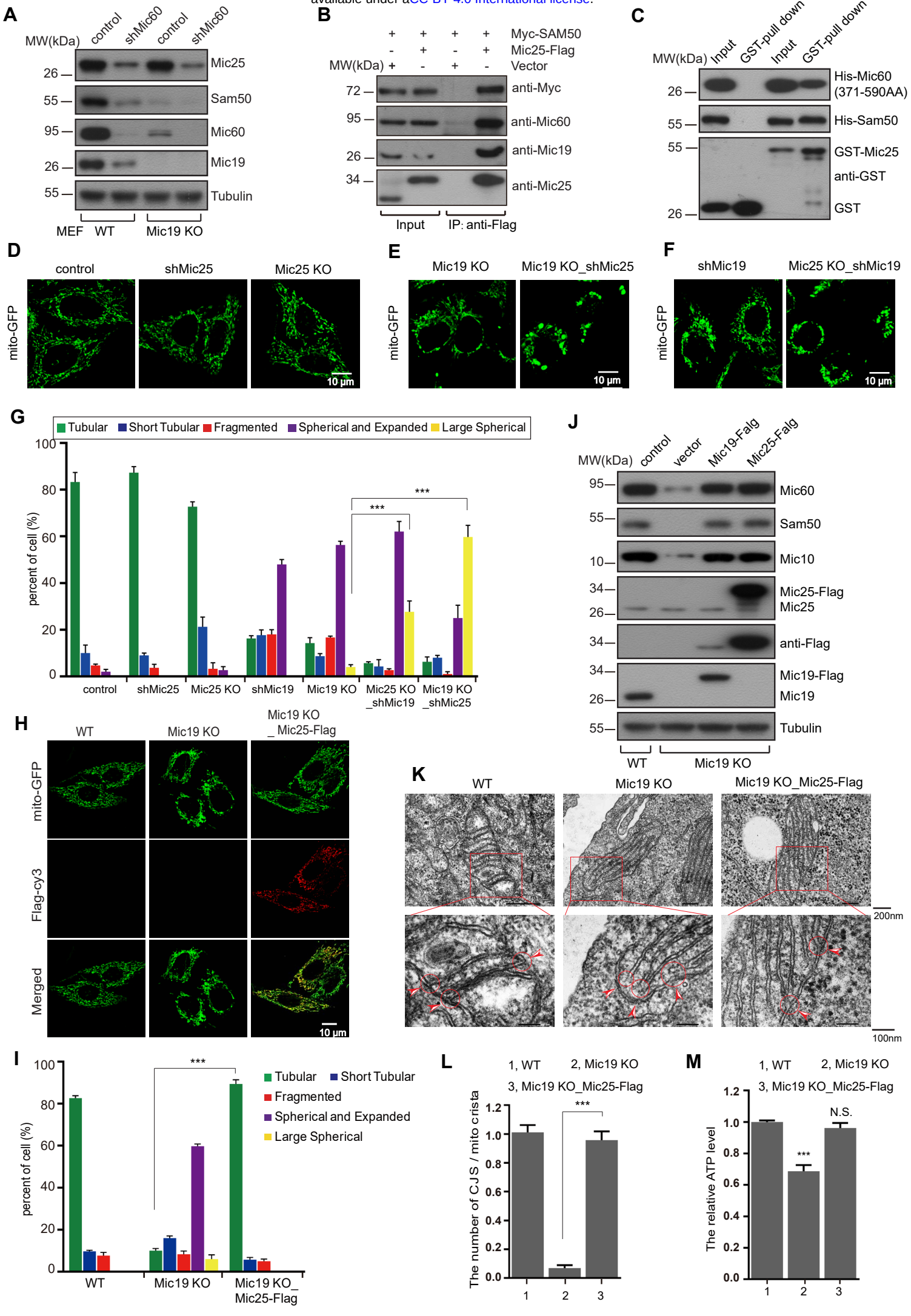

Figure 7

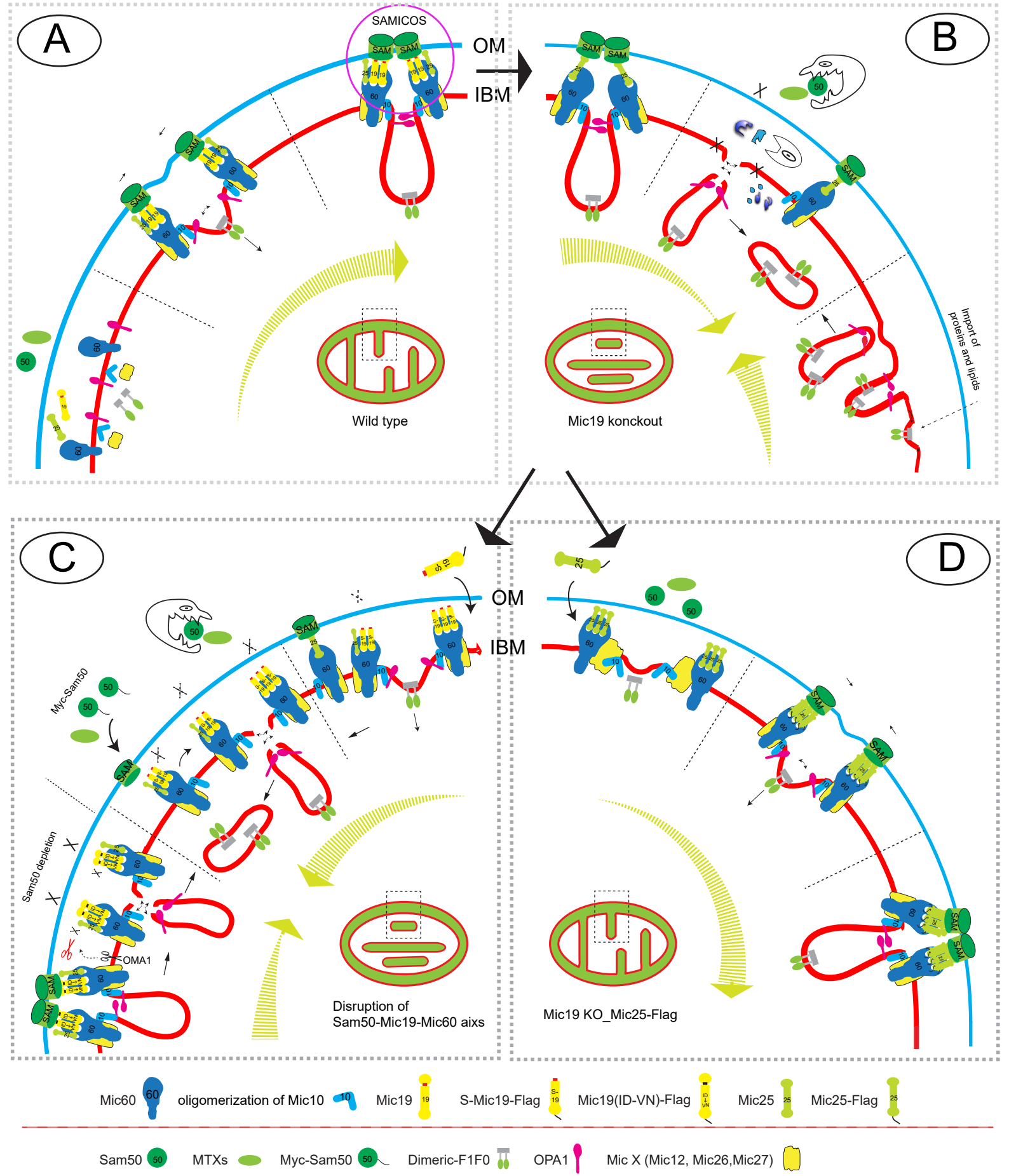

Figure S1

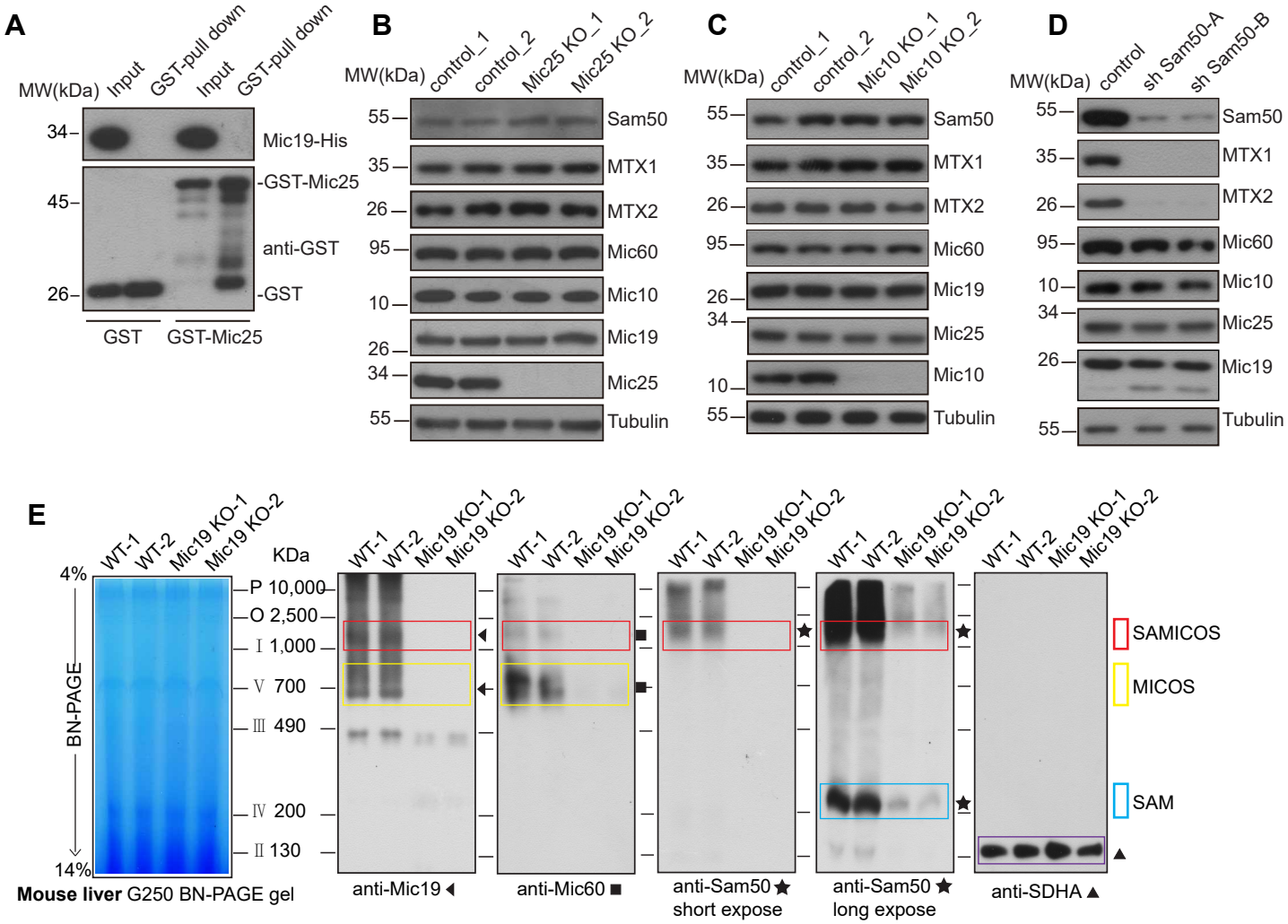

Figure S2

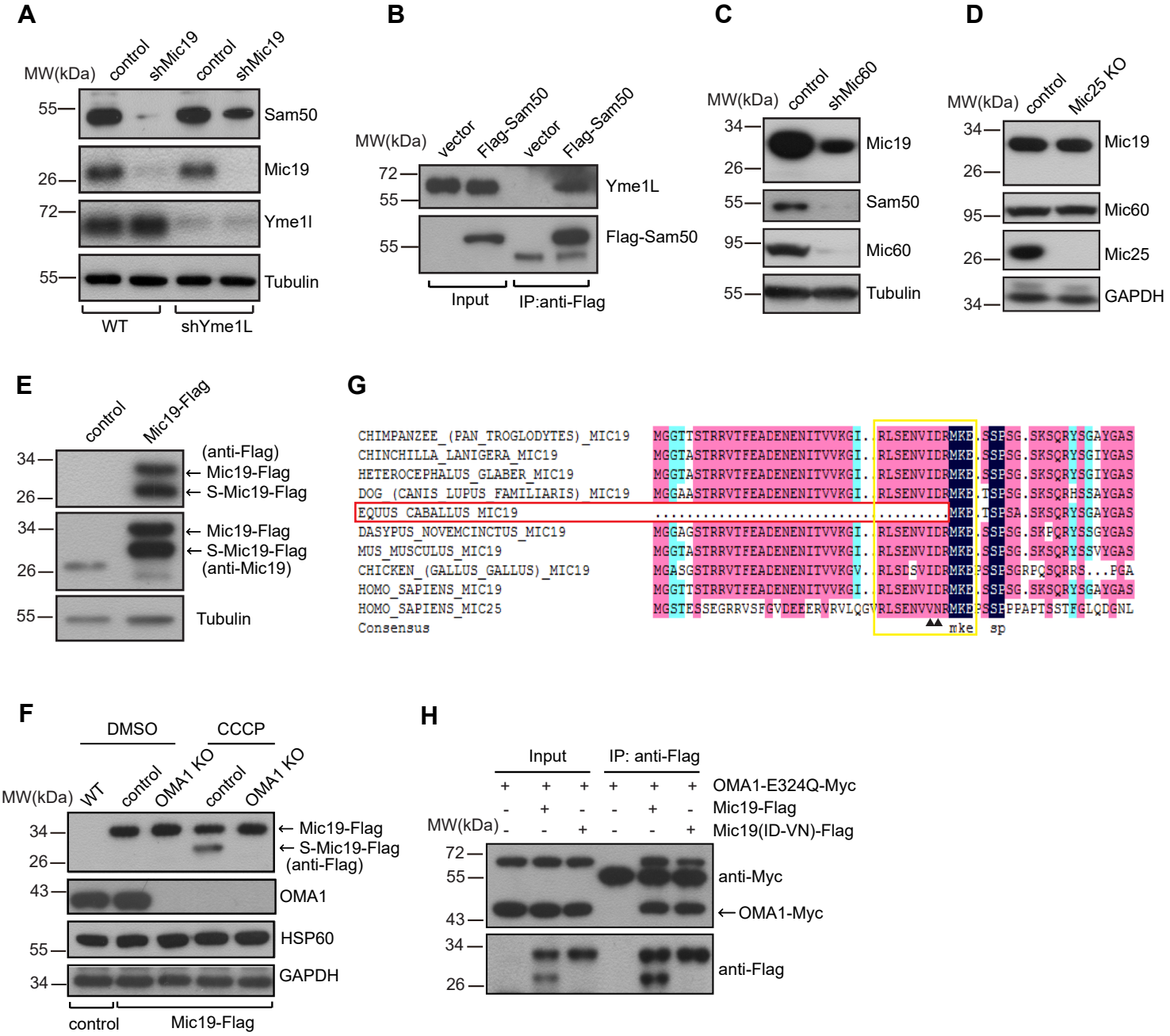

Figure S3

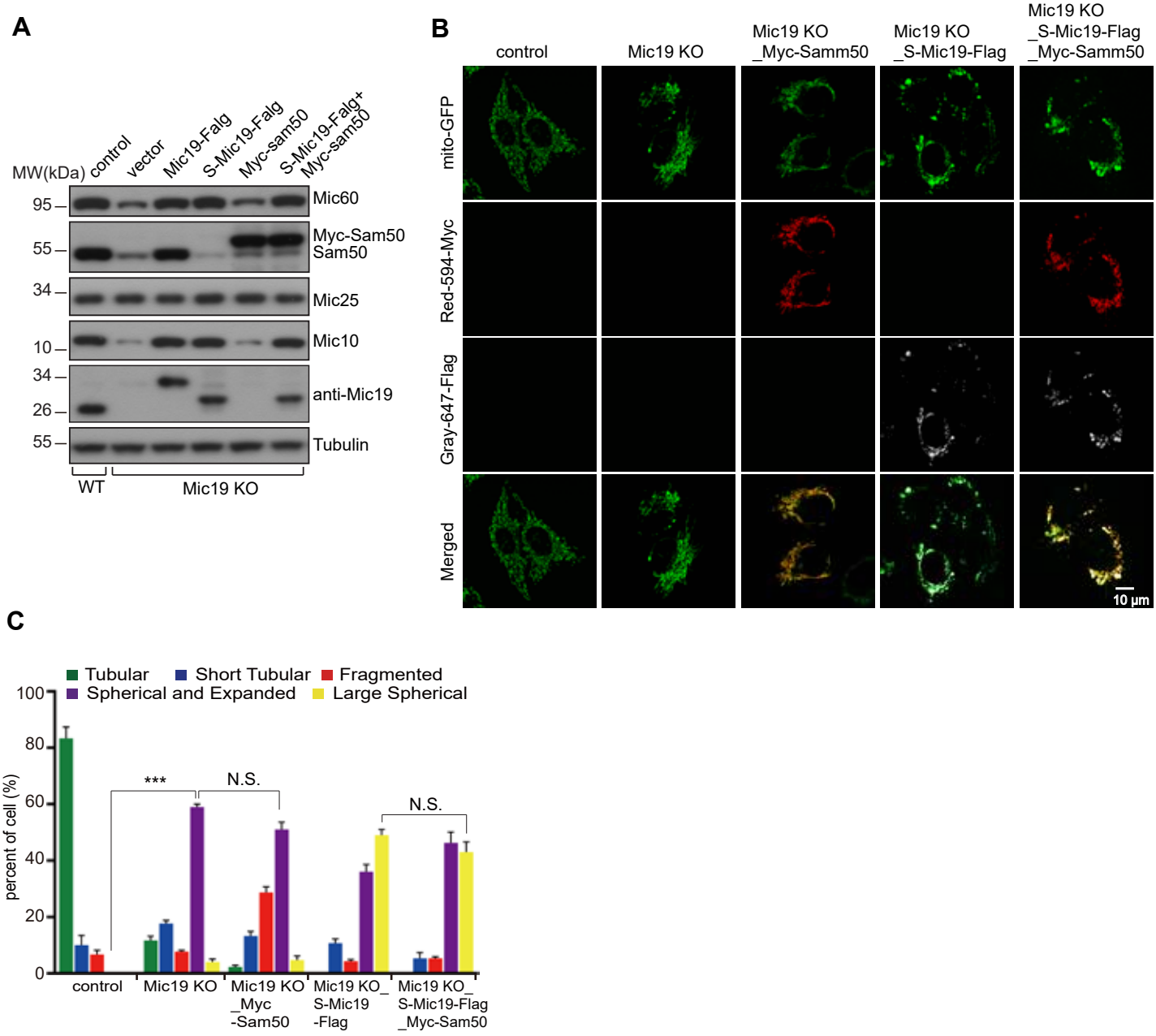

Figure S4

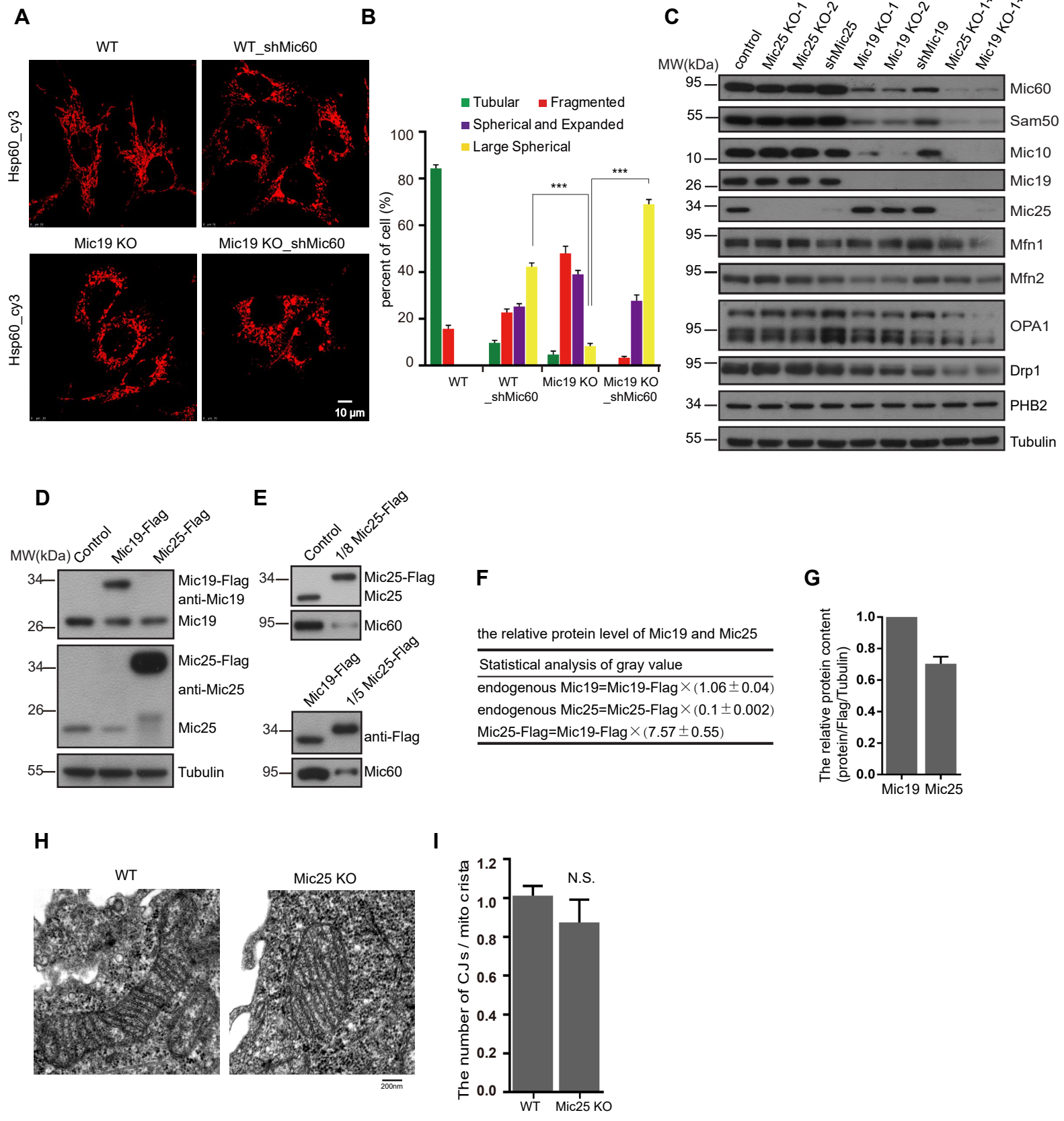

SUPPLEMENTARY INFORMATION

MATERIALS AND METHODS

Western blot, Co-immunoprecipitation and GST-pull down assay

Western blot, Co-immunoprecipitation and GST-pull down assay were performed as we have described previously (Li et al., 2016). All the GST- or His-tagged protein in this study induced with the condition: E. coli BL21 cells were transformed GST- or His-tagged plasmid cultured at 37℃, shaking 200 rpm/min 20-24h, then take 500μl of bacteria solution to inoculate into 10ml LB liquid medium at 37℃, shaking 220 rpm/min about 2~3h. When the optical density reaches (OD600=0.6), the E. coli induced with 0.4mM~1mM IPTG at 16℃, shaking 200 rpm/min 18-24h.

Isolation of mitochondria and BN-PAGE analysis

Homogenization of cells or tissues and solubilization of mitochondria for BN-PAGE were performed according to the protocol (Wittig et al., 2006). We optimized the procedure for isolation of HeLa cells mitochondria: a 100-mm dish of ~90% confluent cells was digested and collected in a 2.0ml EP tubes , and the cell pellet re-suspended in cell homogenization buffer (83mM sucrose, 6.6mM imidazole/HCl, pH 7.0), then ultrasonic disrupt cell membranes on ice with the condition(1% Power, hit 1s, stop 4s, one minute in total). Centrifuge for 10 min at 700g to clear unbroken cells or cell nucleus, and the supernatant subsequently was centrifuged for 5 min at 10000g to collect the pellet containing the crude mitochondria. The pellet further re-suspended and centrifuge for 10 min at 10000g to collect the mitochondria. Isolated mitochondrial were re-suspended in solubilization buffer A (50mM sodium chloride, 50mM Imidazole/HCL, 2mM 6-aminohexanoic acid and 1mM EDTA PH7.0 at 4℃) on ice and lysed by the addition of ~2% digitonin for 30min. The samples were separated on 4–14% blue native polyacrylamide gels. The gel was transferred to PVDF and immunoblotted with the anti-Mic60, anti-Mic19, anti-Sam50 and anti-SDHA or anti-Ndufb8 antibody respectively.

Plasmids and shRNA construction

The vector including pEGFP-N3, pMSCV-puro, pMSCV-hygro and Phage-puro were used to construct recombinant plasmid. shRNAi against target gene was performed using a modified retroviral vector with the H1 promoter to drive the expression of shRNAs (Chen et al., 2005).

The following target sequences for gene knockdown were used: human Mic19: 5'-GGAGCTCAGAGTTCTACAG-3'; human Mic25: 5'-GACGCCGTGACACCTTCTA-3'; human Sam50-A: 5'-GGTCATCGATTCTCGGAAT-3'; human Sam50-B: 5'-ACATTCACTGAAATCATCT-3'; human Yme1L: 5'-GAGCTCTTCAAAGCATTTG-3'; human OMA1: 5'-GAAGTGCTTTGTCATCTAA-3'; Mouse Mic60: 5'-GGTGGTATCTCAGTATCAT-3'. Retrovirus production, cell infection and selection were performed according to the protocol described previously (Li et al., 2016).

CRISPR/Cas9-mediated gene knockout

CRISPR/Cas9-mediated deletion of Mic19, Mic25, Mic10, Yme1L and OMA1, sgRNA sequences were selected using the MIT CRISPR design tool (http://crispr.mit.edu/) and cloned into LentiCRISPRv2 backbone (Addgene #52961). The following guide sequences were used: human Mic19: 5'- TCGGGAGAGGATATGTAGCG -3'; human Mic25: 5'-CTGATGCTGCCTTCGCCCGT -3'; human Mic10: 5'- TGTCTGAGTCGGAGCTCGGC -3'; human Yme1L: 5'- TGTCCAAGTGTTGGCCCCCG -3'; human OMA1: 5'-ACATTAGCATCCACCTCACG -3'. Lentiviral production, cell infection and selection were performed according to Zhang lab protocol (Sanjana et al., 2014).

REFERENCES

Chen, H., Chomyn, A., and Chan, D.C. (2005). Disruption of fusion results in mitochondrial heterogeneity and dysfunction. The Journal of biological chemistry *280*, 26185-26192.

Li, H., Ruan, Y., Zhang, K., Jian, F., Hu, C., Miao, L., Gong, L., Sun, L., Zhang, X., Chen, S., *et al.* (2016). Mic60/Mitofilin determines MICOS assembly essential for mitochondrial dynamics and mtDNA nucleoid organization. Cell death and differentiation *23*, 380-392.

Sanjana, N.E., Shalem, O., and Zhang, F. (2014). Improved vectors and genome-wide libraries for CRISPR screening. Nature methods *11*, 783-784.

Wittig, I., Braun, H.P., and Schagger, H. (2006). Blue native PAGE. Nature protocols *1*, 418-428.